Journal of the European Ceramic Society 20 (2000) 867–888

Heat treatment induced phase and microstructural development in bulk plasma sprayed alumina

R.J. Damani [a,*], P. Makroczy [b]

[a] Department of Structural and Functional Ceramics, University of Leoben, A-8700 Leoben, Austria
[b] Department of Materials Science, Technical University of Košice, 04385 Košice, Slovakia

Received 2 December 1998; received in revised form 20 July 1999; accepted 8 August 1999

Abstract

The influence of systematically varied heat treatments on the microstructure and phase system of a bulk plasma sprayed alumina has been investigated by applying conventional electron microscopy [scanning electron microscopy (SEM) and transmission electron microscopy (TEM)], X-ray and electron diffraction [X-ray diffractometry (XRD) and selected area electron diffraction (SAED)], Archimedean porosimetry and dilatometry. Plasma sprayed alumina has a quasi-laminated microstructure, consisting of layered "splats" with a pronounced ultra-microstructure which results from rapid cooling. The as-sprayed material consists of transition aluminas and about 35% α-Al_2O_3. Both transition phases and α-Al_2O_3 form splats with transversal ultra-fine columnar intra-splat grains. Post deposition exposure to high temperatures causes significant microstructural, phase and dimensional changes. The transition aluminas undergo a continuous order–disorder transformation until the reconstructive phase change to α-Al_2O_3 is reached. This is accompanied by precipitation of aligned porosity, opening of splat interfaces and the formation of dislocation networks. It is suggested that the increase in porosity is responsible for the directionally dependent and lower than expected shrinkage on transformation. Thermal expansivity at lower temperatures is found to be independent of splat orientation. A block domain structure and extensive twinning form during the transition transformations. Extended exposure to near-sintering temperatures leads to the recrystallisation of the splat substructure whilst maintaining the splat structure.

Keywords: Al_2O_3; Electron microscopy; Microstructure-final; Phase transformations; Plasma spraying

1. Introduction

Plasma sprayed ceramics are finding increasing acceptance in various fields of engineering, medicine and industry, ranging from their application as thermal barrier and wear resistance coatings to functioning as bio-active interfaces for medical implants. They are even finding application as free-standing components, such as tubes, pipes and guides, where use of conventional ceramic components has been rejected for reasons of economy, lack of damage tolerance or low resistance to thermal gradients.[1–4] This is not surprising when the various advantages they can bring are considered. Plasma sprayed ceramics are relatively easily worked and formed and deposit thickness may be varied from tens of micrometres for coatings to tens of millimetres for free-standing components. Various composite systems may be deposited and both coatings and free-standing components can exhibit high crack resistance and thermal shock resistance; indeed, free-standing alumina components have been shown to withstand thermal shocks in excess of 1000°C, without appreciable deterioration in strength.[5,6]

The various properties of plasma sprayed ceramics, and especially the differences from conventionally sintered ceramics, are known to be dependent on their anisotropic, quasi-laminated, "splat" microstuctures and non-equilibrium phase compositions.[7,8] These microstructures are very dependent on the external parameters of spraying, e.g. arc current, carrier gas pressure, gun-substrate distance, etc. Variations in these parameters can lead to large changes in microstructure and phase system and hence to great variations in the properties of the deposited ceramic.[1,2] For any given as-sprayed coating-property system, the spraying parameters have to be specifically and empirically optimised. Post-production thermomechanical loading and especially exposure to high temperatures can, however, lead to

* Corresponding author. Tel.: +43-3842-402-9112; fax: +43-3842-402-9102.
E-mail address: damani@unileoben.ac.at (R.J. Damani).

0955-2219/00/$ - see front matter
PII: S0955-2219(99)00217-4

extensive changes in the properties of ceramic systems. These are related to changes in the internal structure, and/or the phase composition.[6,8–10] For instance, it has been reported that the plasma sprayed alumina system can be subject to considerable creep, even at relatively low temperatures and stresses.[5] However, it is also known that the as-sprayed alumina system often contains a considerable amount of metastable γ-Al_2O_3, and this transforms, through a series of intermediate (transition) phases, to the room temperature stable α-Al_2O_3 phase.[11–14] This sequential transformation, which must be accompanied by microstructural changes, is likely to be a major cause of the observed creep effect.

If understood and optimised, this ability to vary microstructure and properties may prove advantageous and it may become possible to age plasma-sprayed ceramic deposits. This is done at present in some systems, especially the alumina system, e.g. the thermal ageing of freestanding alumina components, or in-situ treatments by post-spray passes of the plasma flame over a deposit surface, but the heat treatments applied are generally arbitrary and designed to result in the conversion of metastable phases, or to induce post deposition sintering. A deeper understanding of the nature of the microstructure and the changes resulting from heat treatment is required if a systematic attempt is to be made to engineer optimal material properties.

Much work has been done to characterise the complex structures which form in plasma sprayed ceramic deposits. Alumina and alumina related systems, being commercially important and well studied in their conventional sintered forms, have received particular attention (see, e.g. Refs. 15–23). The majority of research has been carried out on deposits close to the interface with the substrate and macro-features of the microstructure, e.g. splat shape, distribution alignment and intersplat interfaces. Relatively little has been published on the micro or nanoscale substructures (ultra-microstructures, e.g. splat internal grain configuration, pore type, morphology and distribution) of plasma sprayed ceramic coatings or bulk matrial. Such investigations, in general, require the application of transmission electron microscopy (TEM) and related techniques (see, e.g. Refs. 24–29). The scope of such studies is often limited by the various difficulties of preparing suitable thin foils from the fragile deposits, the tedious and time consuming nature of such investigations and by a tendency to concentrate on specific crystallographic details. Furthermore, although it is well known that plasma-sprayed alumina deposits often contain a large proportion of metastable phases, the transformations of which have received considerable attention in conventional aluminas, there has been relatively little systematic investigation of the time and temperature related development of their phase system coupled with the evolution of their various substructures. Microstructural substructures and the phase system must play dominant roles in the stability, mechanical behaviour and chemical activity of these materials, and as such are attracting increasing research interest (see, e.g. Refs. 20, 30 and 31).

It has, therefore, been the objective of this work to systematically investigate and provide a comprehensive overview of phase, structural and sub-structural development in the microstructure of a bulk plasma sprayed alumina as it evolves under the influence of various heat treatments.

2. Methods and techniques of investigation

2.1. Material

The alumina material used in this investigation was atmospheric plasma spray (APS) deposited by LWK Plasmakeramik, Gummersbach, Germany, using a water stabilised arc plasma gun. It was sprayed from a commercially available powder agglomerate (Alcoa CT100, 99.5% α-Al_2O_3, median agglomerate granule size: 92 μm, with individual crystallite size between 2 and 5 μm) (Fig. 1) in 18 passes onto a removable steel mandrel, to form a free-standing tube with wall thickness of about 80 mm. The as-sprayed material had a porosity of about 13%.

Samples were cut from the bulk to minimise substrate influence. An overview of the microstructure through cross sections of as-sprayed and fully heat treated materials (as described later) is given in the scanning electron microscopy (SEM) micrographs in Fig. 2. The typical splat structure is dominant in both material conditions.

2.2. Heat treatments

Two series of heat treatments were carried out. In the first, blocks of material were heated at 5°C/min and held at constant temperature for 12 hours at 900, 1050, 1180 and 1550°C, and then furnace cooled to room temperature. These temperatures were chosen on the basis of the transformation temperatures for the various metastable

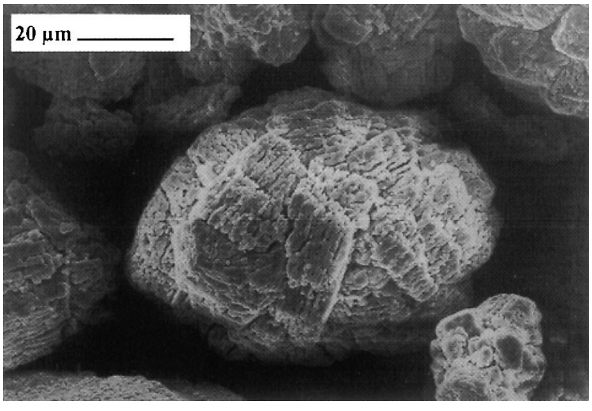

Fig. 1. SEM photo-micrograph of sprayed alumina powder agglomerate.

alumina phases, given in literature.[11,12] The last heat treatment is just below the common sintering temperature for high alumina materials,[32] and is similar to treatments applied in industry to consolidate and make thermally stable sprayed products.

A second series of heat treatments was based on the outcome of the investigation by dilatometry (described below). This showed the first major dimensional instability to be at about 1180°C at a heating rate of 5°C/min. Consequently, a series of samples was heated in fan assisted furnaces to 1180°C at 20°C/min, and held at this temperature for different times up to 12 h before furnace cooling to room temperature (RT). The faster heating rate was applied to minimise the time spent in the dynamic part of the cycle.

2.3. X-ray diffractometry, dilatometry and thermo-gravimetric analyses

Phase analysis was conducted by X-ray diffractometry (XRD) using a Siemens D-500 diffractometer with CUK_α radiation ($\lambda = 1.542$ Å). Solid samples were used as preliminary X-ray investigations had shown that there was no identifiable crystallographic texture,[6] and a control powder measurement had shown no appreciable difference to the solid measurements. Measurements were made primarily on samples taken from the bulk. One measurement was made on the substrate-deposit interface layer to examine the differences to the bulk material.

Thermal dimensional stability measurements were made on small beams of as-sprayed material using a Netzsch 412 E horizontal push-rod dilatometer. The samples were heated in a graphite chamber with static air at 5°C/min. Measurement instabilities were accounted for by calibration against a standard sintered alumina. The samples were cut from the as-sprayed cylinder in three orthogonal directions as shown in Fig. 3: radial, i.e. so that the long axis of the beam was normal to the splats, axial, i.e. along the axis of the sprayed cylinder and tangential. In the case of both axially and tangentially cut samples the long axis of the cut samples was essentially parallel to the alignment of splats.

Simple thermal gravimetric analysis (TGA), to check for rapid weight loss during the heating cycle as would be expected from dehydroxylation of the material, was conducted using Netzsch STA 409 C simultaneous thermal analyses equipment. A 105.5 mg powder sample was heated in an alumina crucible in static air at 5°C/min.

2.4. Porosimetry

Archimedean porosimetry was used to quantitatively follow the evolution of porosity with heat treatments. Samples were immersed in water and left to soak under light vacuum to facilitate pore penetration. Samples were weighed after overnight immersion and after 72 h immersion. The weight of the samples was measured immersed in water, wet but out of water, and after extended drying at 100°C. Porosity was estimated from the assumed theoretical density and the following set of relationships:

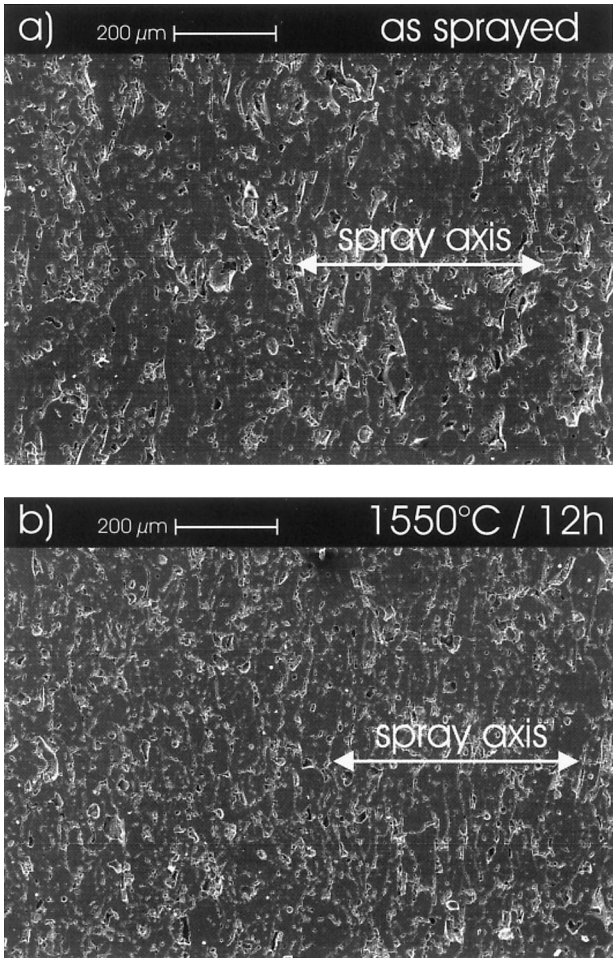

Fig. 2. SEM micrographs of (a) cross-section through as-sprayed material. The typical splat structure is clearly visible, and (b) material heat treated at 155°C for 12 h. The splat structure is still clearly dominant, but porosity appears to have increased.

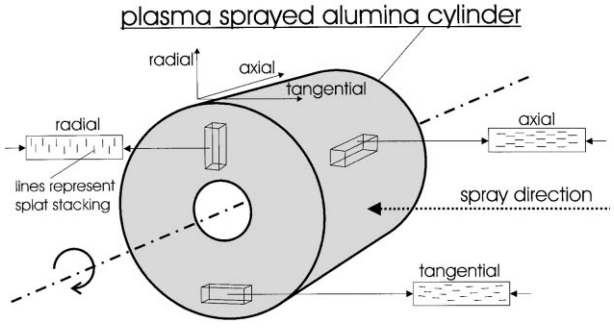

Fig. 3. Schematic representation of the orientation of samples removed from the sprayed thick-walled cylinder. The short lines in the samples represent the stacking sequence of splats.

$$P_o = [(W_w - W_d)/(W_w - W_{uw})] \times 100, \quad (1)$$

$$P_c = \left[1 - \rho_{(c+o)}/\rho_{th}\right] \times 100 - P_o, \quad (2)$$

$$P_t = P_c + P_o, \quad (3)$$

$$\rho_{(c+o)} = [W_d/(W_n - W_{uw})] \times \rho_w, \quad (4)$$

where W_d is the weight of the dry sample, W_w is the weight of the sample wet but out of water, W_{uw} is the weight of the sample under water, $\rho_{(c+o)}$ is the density of the sample (including open and closed porosity), ρ_w is the density of water at the temperature of testing, ρ_{th} is the theoretical density of the alumina, P_o is the percentage of open porosity, P_c is the percentage of closed porosity and P_t is the total percentage of porosity. The theoretical density of the as-sprayed material was calculated using a simple rule of mixtures from X-ray data: after preliminary pole-figure measurements failed to provide evidence of crystallographic texture in a previous investigation, an estimate of the phase composition of the as-sprayed material was made by applying the integrated intensity method to selected peaks in the traces of one sample, in the as-sprayed state and after conversion to 100% α-Al_2O_3. The as-sprayed material was found to contain about 35% α-Al_2O_3, and 65% γ-Al_2O_3[6] (the other transition aluminas were omitted in this estimation due to the percentage fractions and the difficulty of distinguishing them from the γ-Al_2O_3). Due to lack of consistent literature data, the assumption was made that the theoretical densities of the transition aluminas do not differ greatly from those of γ-Al_2O_3.

2.5. TEM investigation

The selection of material for samples for TEM investigation was made on the basis of post heat-treatment X-ray diffraction. Samples were chosen that revealed significant phase change. Thin foil specimen were prepared by slightly modifying standard techniques of ceramic foil preparation. A cylinder of material 2.3 mm in diameter was cut out of each heat treated block and mounted into a hollow brass tube using glue. The glue plays a vital part in the preparation, as it penetrates into the open pores and interfaces and provides reinforcement during subsequent stages of preparation. Thin slices were then cut from this tube, ground until plan-parallel and polished and mechanically dimpled from one side. The sample was ion beam milled using ionised argon, at an angle of attack of 3° to perforation. It was then sputtered with a thin coat of carbon. The samples were observed in a Jeol 2000FX TEM operating at 200 kV.

3. Results

3.1. X-ray diffraction

There was a substantial difference in the X-ray trace of as-sprayed alumina material from the substrate–deposit interface and material from the bulk. The interfacial material was largely γ-Al_2O_3 and α-Al_2O_3 (trace not shown here) and showed considerably less evidence of the development of δ-Al_2O_3 or θ-Al_2O_3 than the bulk material, indicating higher cooling rates, or less reheating by subsequent torch passes and deposition.

In-depth investigation showed little variation in relative amounts of the different phases, indicating that once a certain depth of deposit had built up, the cooling rate did not change dramatically. The bulk as-sprayed material showed evidence of the coexistence of α, γ and δ-Al_2O_3.

The traces from samples which underwent isothermal heat treatments at different temperatures for 12 h are shown in Fig. 4, and show the progressive development of the transition aluminas. It is clearly seen that many of the peaks of the various aluminas overlap, thus making positive identification of a phase by the exclusion of others difficult. The development of the tetragonal δ-Al_2O_3 phase is already clear in the material heat treated at 900°C, but it is most obvious in the material after 12 h at 1050°C. Theta alumina may just be identified after heat treatment at 1050°C, but is clearly present as a minor phase in the material heat treated at 1180°C. By far the greater part of the material heat treated at 1180°C is alpha alumina. After 12 h at 1550°C, the material may be considered to be 100% α-Al_2O_3. It should be noted that the traces shown originate from different samples. Hence, the absolute intensity levels should not be compared between traces. However, relative peak intensifies may be used as a guide to phase development within any one trace. The JCPDS standards 43-1484 (α-Al_2O_3), 29-0063 (γ-Al_2O_3), 16-0394 (δ-Al_2O_3) and 23-1009 (θ-Al_2O_3) were found to correspond most closely with the measured traces and were used for peak identification.

Fig. 5 shows the traces for material heat treated isothermally at 1180°C for different times. The traces show a similar phase development to the materials heat treated at different temperatures. After 10 min at this temperature the phase composition is clearly similar to that after 12 h at 900°C, and after 20 min there is similarity to that heat treated for 12 h at 1050°C. The amount of transition alumina is already reduced after 90 min and the material may be considered as consisting of almost entirely α-Al_2O_3 after 12 h, although a minor content of θ-Al_2O_3 may still be identified.

Note, for simplicity, not all peaks have been labelled in Figs. 4 and 5. Unlabelled peaks correspond to peaks above or below them, e.g. in Fig. 4 all peaks at about 26° are α-Al_2O_3.

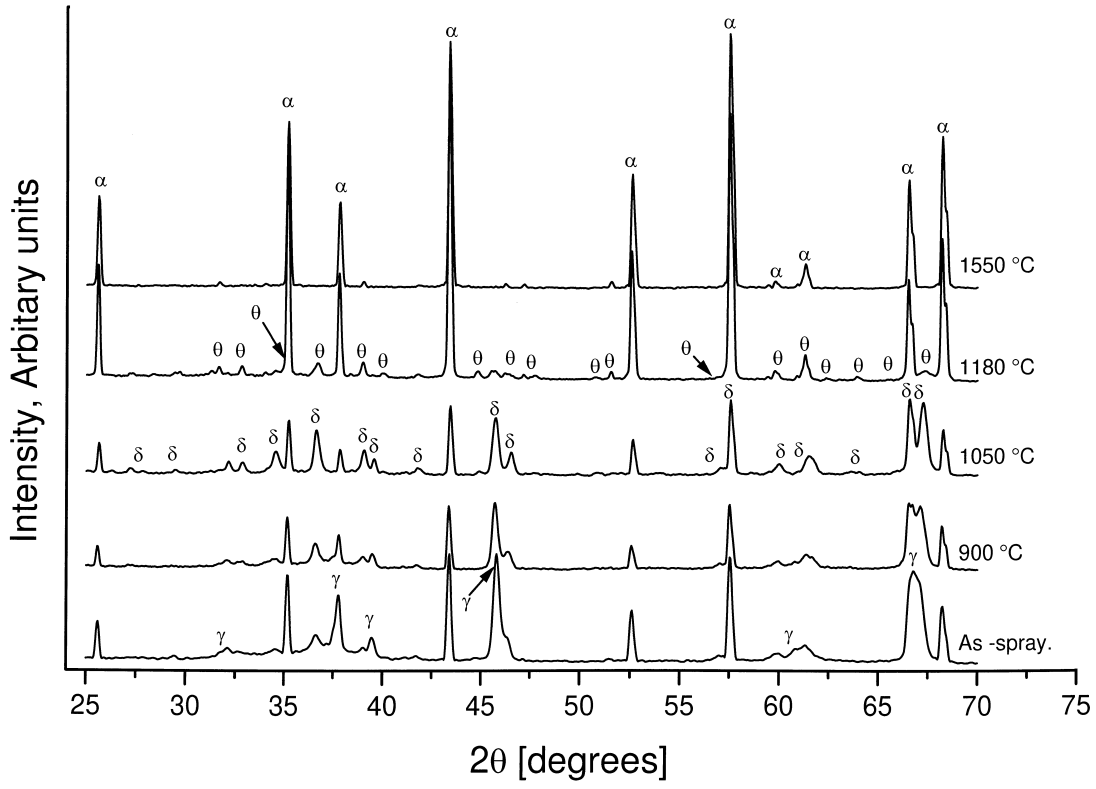

Fig. 4. X-ray diffraction traces showing phase development from the as-sprayed state for plasma-sprayed alumina annealed for 12 h at various temperatures.

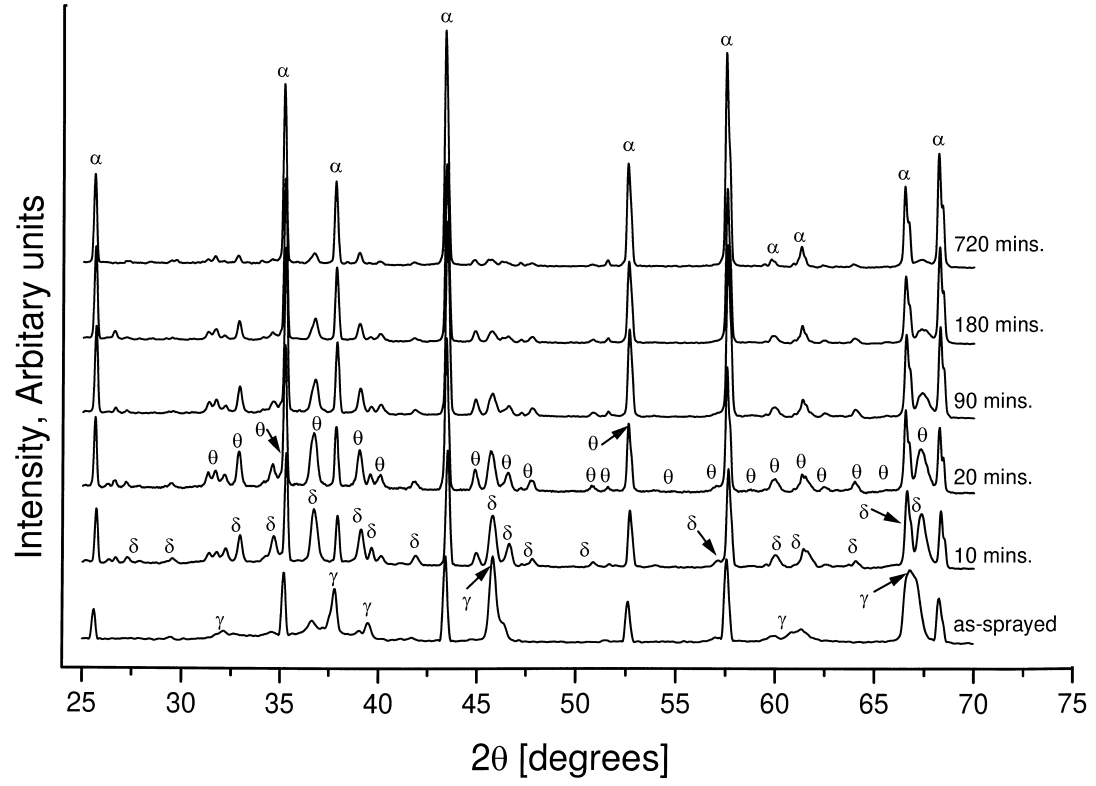

Fig. 5. X-ray diffraction traces showing phase development in plasma sprayed alumina heat treated at 1180°C for different times.

3.2. Dilatometry and TGA

Dimensional changes on heating may be seen in Fig. 6, which shows the changes on one heating cycle at a heating rate of 5°C/min. For simplicity only the axial and radial samples are represented as the tangentially cut sample behaved almost identically to the axial sample. The expansion curves are almost indistinguishable in both directions from room temperature up to about 1000°C, yielding a coefficient of thermal expansion in both cases that ranges between 4.5×10^{-6} and 8×10^{-6} K^{-1} for temperatures between 200 and 1000°C. It is difficult to exactly identify the point of divergence of the two readings, but this lies between 900 and 1000°C and corresponds to the γ-Al_2O_3 to δ-Al_2O_3 ordering transformation. There is evidently a slow down in rate of expansion above 1000°C, followed by a rapid shrinkage at about 1200°C. This shrinkage is attributed to the transformation to α-Al_2O_3. A permanent volume contraction of approximately 3 to 3.5% was determined after cooling to room temperature by measuring sample dimensions with a micrometer screw gage.

The striking feature of the dilatometry curves is the difference in shrinkage in the orthogonal directions. The axial and tangential directions are found to be subject to the same shrinkage (approx. 0.66% linear contraction), but the radial direction shrinks about 60% more (approx. 1.05%). Furthermore, the maxima of the curves occur at different temperatures in the different directions: about 1215 and 1190°C for axial and radial specimens, respectively.

After the main transformation the dilatometry curves again show material expansion up to about 1400°C, after which there is a little further shrinkage. Thus it may be inferred that macroscopic sintering effects do not occur until at least 1400°C. Thermal expansion on cooling from 1550 to 700°C yielded a thermal expansion coefficient of 9.9×10^{6} K^{-1}, which corresponds well to the thermal expansion coefficient of conventionally sintered α-Al_2O_3 at elevated temperatures.[12,33]

Simple TGA analysis showed a rapid mass reduction of about 0.4% between 100 and 500°C. This loss is low considering that according to literature there is between 3.4 and 7.5% surface and lattice tied water in γ-Al_2O_3,[11,34,35] (which would correspond to a loss of up to 2.2 and 4.9% in our material, respectively). It is assumed that this mass loss corresponds to dehydroxylation, i.e. the driving off of tied lattice water, of γ-Al_2O_3.

3.3. Porosimetry

The results of Archimedean porosimetry are summarised in the graph in Fig. 7. The overall amount of porosity changed little up to the temperature of reconstructive transformation. This phase change is accompanied by a fairly large jump in both open and especially

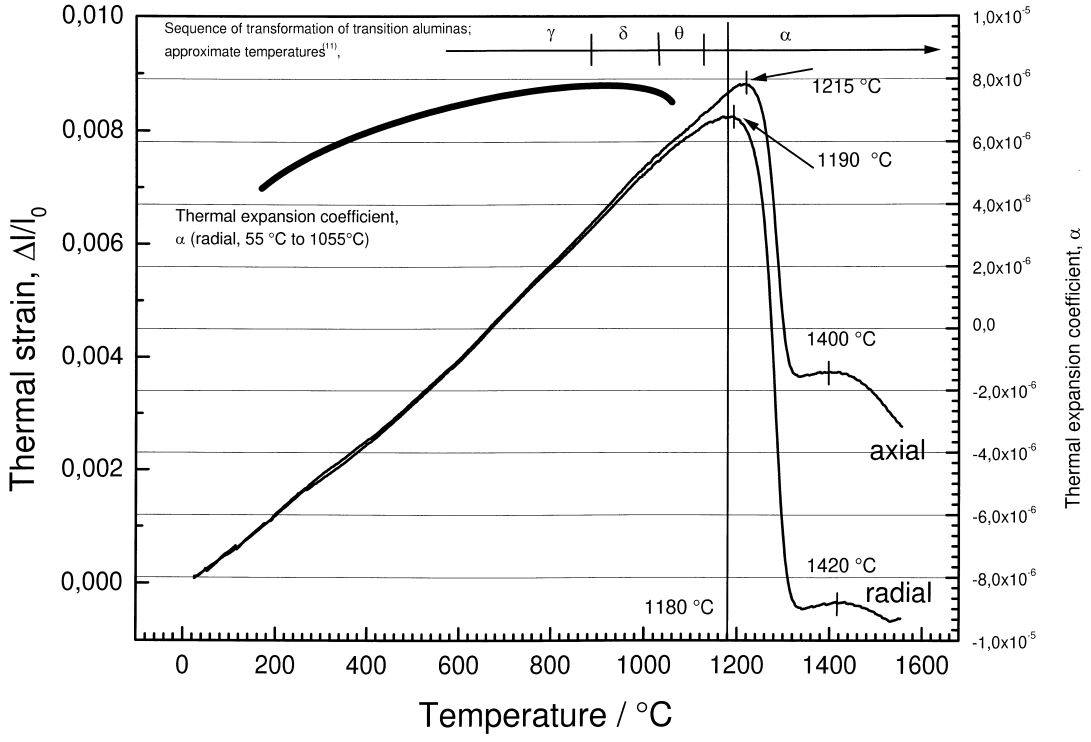

Fig. 6. Dilatometry: dimensional changes in plasma-sprayed alumina in the two principle inicrostructural orientations on heating at 5°C/min. The sequence of expected phase transformations is indicated at the top of the figure (the thermal expansion coefficient curve was obtained by smoothing the measured data points).

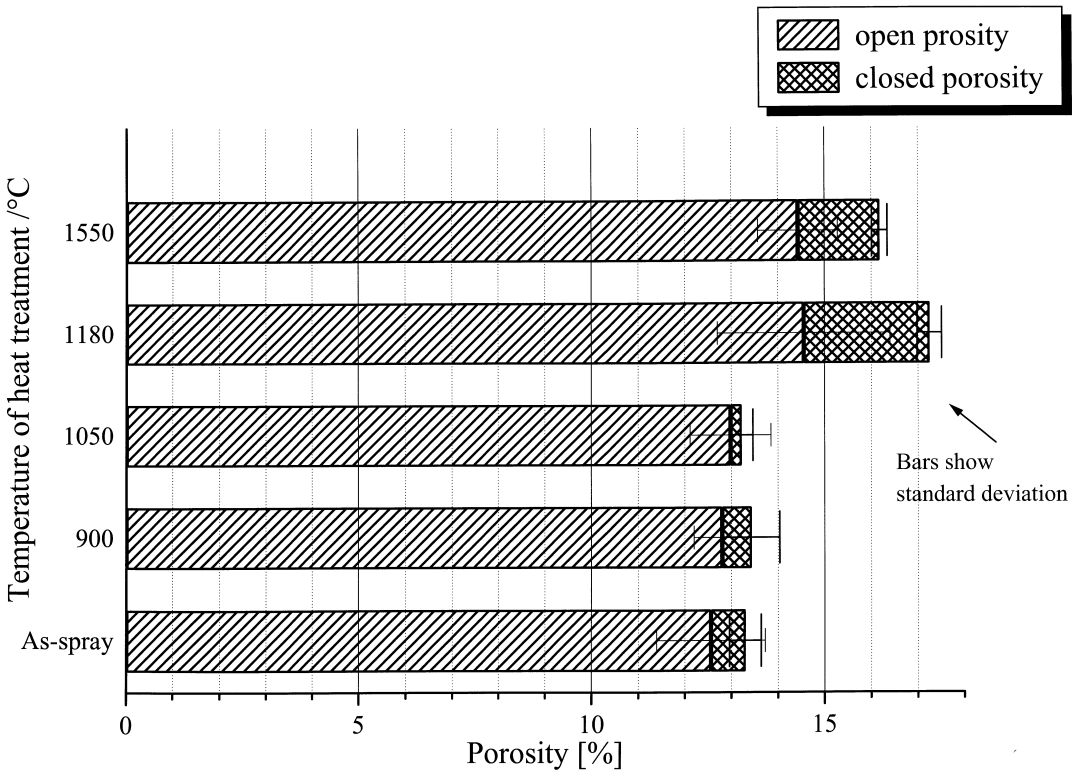

Fig. 7. Graph showing results of Archimedean porosimetry in as-sprayed and 12 h heat treated materials. The samples were immersed in water for 72 h.

closed porosity. The total amount of porosity recedes a little after the higher temperature (i.e. 1550°C) heat treatment. Most of this reduction is due to a decrease in closed porosity.

It is important to be aware of the dramatic effect a variation in immersion times can have on accuracy and scatter. Short immersion times are sufficient to estimate the total porosity, but very long immersions are required if reasonable estimates of the fractions of open and closed porosity are to be made. For example, 4.5% closed porosity out of a total porosity of 13% was determined in samples of as-sprayed material immersed for 6 h. After immersion for 3 days, the total amount of closed porosity determined had reduced to less than 1% whilst the total amount of porosity stayed effectively unchanged at 13.5%.

3.4. TEM and SAED investigation

When presenting and analysing the results of a TEM investigation, one should bear in mind the relatively small volume of material actually examined, and whether or not the results can be evaluated as being representative. The TEM investigation of this plasma sprayed material is further complicated by the fact that the microstructure is inherently heterogeneous. Hence, it is not always easy to separate the inherent effects of deposition, from the consequences of heat treatment. Accordingly, in the following, only features that were deemed to be typical of the microstructure and a consequence of the appropriate thermal history of the material have been reported.

3.4.1. The as-sprayed material

Metallographic sectioning shows powder particles are deposited as splats in various sizes and with varying degrees of flattening. Some original powder particles have not been melted at all (or only melted a little on the outer surface) and are found as complete spherical agglomerates within the microstructure. These account for some of the α-Al_2O_3 found in the X-ray traces.

TEM investigation revealed that the deposited splats have a columnar internal substructure (ultra-microstructure). The columns have a width between 0.2 and 1 μm, which is reminiscent of directional solidification, or the beginning of dendritic solidification (see Figs. 8 and 9). The columns in a splat are always initially oriented perpendicularly away from the interface of impact with the previously deposited splat. This is identifiable because gas from the plasma envelope, trapped at the impinging surface by the next viscous/molten impacting particle, results in a mottled surface (Fig. 9). In contrast, the opposite surface is always smooth, indicating that the splat had completely solidified by the time of impact of the next molten particle. After initially running perpendicular to the surface of impact, the direction of the columns may change (they do not necessarily run perpendicularly throughout the splat), indicating the columns form

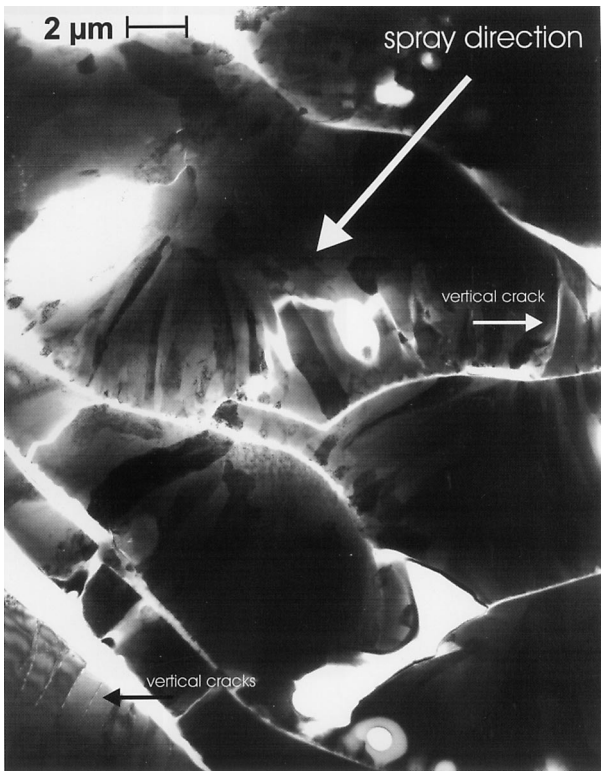

Fig. 8. TEM micrograph showing clearly the splat internal columnar substructure of the majority of as-sprayed splats. Impingement zones between the individual columns, agglomeration of porosity and vertical cracks are clearly visible.

Fig. 9. TEM micrographs of splat internal structures at higher magnification. Large spherical intrasplat and hemispherical interfacial pores resulting from entrapped gasses during solidification are evident.

according to the path of the heat flux out of a splat as it cools.

The columns themselves often appear to have weak interfaces between one another, as may be inferred from the vertical cracking frequently observed between them. The weakness of the interfaces may be due to crystallographic mismatch between neighbouring columns in some cases. In others, it is clearly a result of the agglomeration of porosity (see bottom left of Fig. 8). The contrast on the TEM images from neighbouring columns within splats indicates that they have different crystallographic orientations. This is confirmed by selected area electron diffraction (SAED) across columns.

Higher magnifications revealed that these columns consist of a group of finer sub-columns (between 50 and 200 nm wide) which share the same crystallographic orientation, but are separated by fine, continuous intracolumnar porosity reminiscent of the segregation of point defects or dissolved gas on rapid solidification (see Fig. 10(a)). The SAED pattern in Fig. 10(b) is taken from across these three lamellae and shows clearly that all three share the same crystallographic orientation. This intracolumnar porosity appears more pronounced in larger splats, i.e. where cooling rates were presumably lower, and may have a significant influence on the thermo-mechanical properties and characteristics of the as-sprayed material.

Two other kinds of porosity are also evident in the splats of the as-sprayed material. There are large isolated pores trapped wholly within splats, which arise from gas bubbles trapped in molten particles; and fine, unstructured porosity, randomly distributed, but in relatively high concentration within some splats, which may arise from finely dispersed trapped gas bubbles in the melt (see Figs. 9 and 11). This second type is more common in splats that do not solidify with a columnar structure. However, the grains themselves give well defined electron diffraction patterns indicating they are crystalline.

The smaller splats exhibit columns that proceed all the way through the splat. However, in larger splats columns often proceed into areas of equiaxed grains. This is similar to the chill zone morphology reported by Braue[26] for mullite and spinel plasma sprayed coatings. It is not certain, however, if this morphology is a result of changes in cooling rate and post deposition heating, or whether it is due to nucleation from within the splat, by seed crystallites from the original powder agglomerates. In fact, both columnar and equiaxed grains were identified by selected area electron diffraction in such cases as being α-Al_2O_3.

It has been possible to use SAED to identify both α-Al_2O_3 and near-γ-Al_2O_3 as columnar structures. The near-γ-Al_2O_3 phase was identified only in thin splats with pronounced columnar ultra-microstructure. The SAED patterns in Fig. 12 are from the same column in one splat, but are for different zone axes. The streaking

(a)

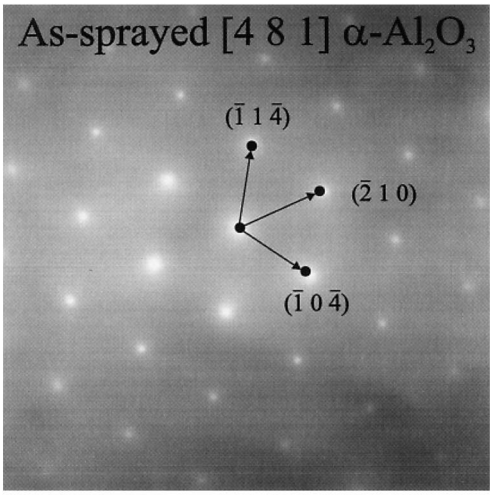

(b)

Fig. 10. (a) TEM micrograph showing subdivision of individual columns by segregation of gas or defects during solidification and (b) SAED pattern taken across all three sub-columns shown in (a). All three sub-columns share the same crystallographic orientation.

in Fig. 12(a) indicates the presence of planar faults, and the positions of the spots agree very well for the [100] of γ-Al_2O_3. The positions of the spots in Fig. 12(b), however, despite coming from the same column, agree very well with the [334] of δ-Al_2O_3. It may be assumed that the γ-Al_2O_3 phase is beginning to undergo the transformation to δ-Al_2O_3, and this column finds itself in an early transition state.

Fig. 11. TEM micrograph showing unstructured porosity in splats without columnar substructure. The splats still give well defined SAED patterns and are therefore crystalline.

3.4.2. After 12 h at 900°C

The X-ray trace for this material shows significant difference to that for the as-sprayed material. There is considerably more δ-Al_2O_3 present, but no discernable increase in α-Al_2O_3. This indicates that a significant amount of γ-Al_2O_3 has transformed into δ-Al_2O_3, as would be expected from the transition alumina transformation series.

Observation of the microstructure after annealing at 900°C for 12 h revealed few major changes from the as-sprayed condition. The columnar substructure of the splats was still clearly visible, as can be seen in the micrograph in Fig. 13. At higher resolutions, however, it became evident that the intracolumnar aligned porosity had become more pronounced throughout the sample. Furthermore, very fine faceted and aligned, but not connected, porosity (indicating compliance with crystal orientation), about 10 to 20 nm in diameter and separated by about 50 nm, was also observed to have formed within the columns (see Fig. 14(a)).

SAED of the columns revealed that a high degree of ordering had developed (Fig. 14(b)). This structure appears to correspond to a phase with a superlattice consisting of triple stacked spinel type cubic cells, in agreement with reported structures for δ-Al_2O_3.[14,36,37] The interconnected streaks through the diffraction spots are probably the consequence of a highly developed stacking fault substructure within the columns.

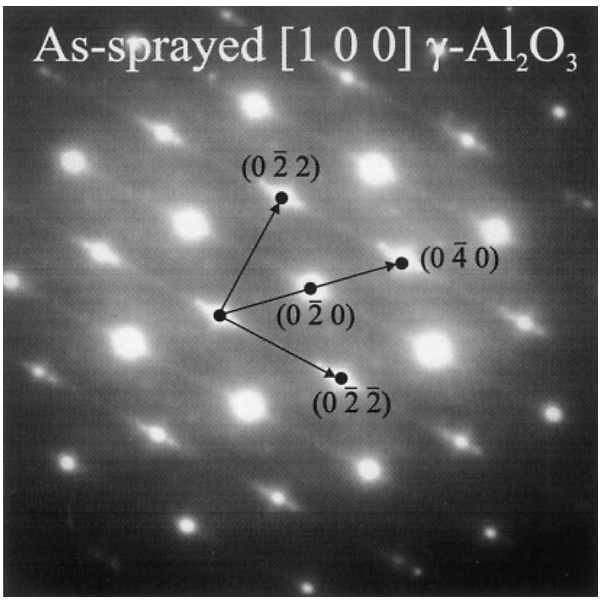

(a)

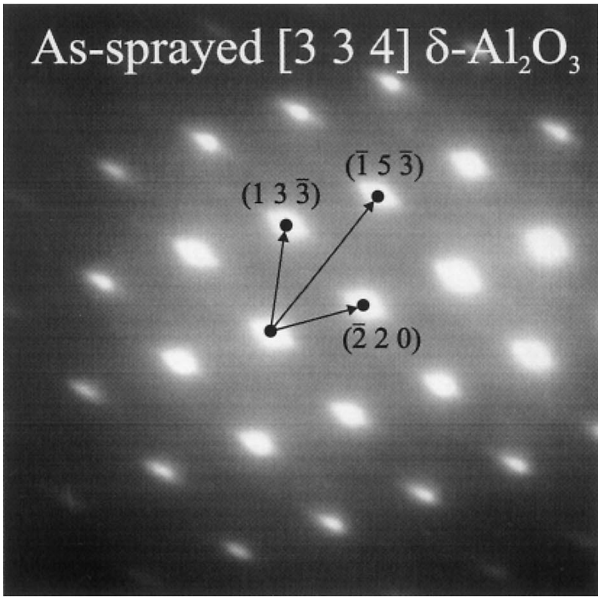

(b)

Fig. 12. SAED patterns from one column in an as-sprayed splat: (a) shows the [100] zone axis of γ-Al_2O_3, the almost continuous streaking indicates the presence of planar faults; (b) is taken from the same column as that indexed in (a). This, however, is best indexed as the [334] zone axis of δ-Al_2O_3.

Incidentally, the high intensity spots on the SAED pattern shown in Fig. 14(b) agree exactly with those in Fig. 12(a) which shows γ-Al_2O_3 in the as-sprayed material (both SAED patterns show the same [100] zone axis), but the low intensity spots between them arise from planes which belong to δ-Al_2O_3, indicating the development of the ordered structure. Furthermore, the streaking which was seen in Fig. 12(a) is strongly developed in the SAED pattern in Fig. 14(b). This provides further evidence that the grain from which the SAED

Fig. 13. TEM micrograph showing internal structure of splats after heat treatment at 900°C for 12 h. The splat internal columnar substructure is still evident. An entrapped incompletely melted original powder particle may be seen in the bottom left.

pattern in Fig. 12(a) was taken was in an intermediate stage of the γ-Al_2O_3 to δ-Al_2O_3 transition.

At the bottom of Fig. 13 an incompletely melted original powder particle is clearly visible. There is obviously a large amount of trapped gas at the interface with the next impinging splat. Although not universal, this type of interface was very common for such powder-splat configurations. It is an interesting feature, however, that despite the lack of contact between the powder and impinging splat, the columnar internal structure has formed unperturbed.

3.4.3. After 12 h at 1050°C

Material heat treated at 1050°C for 12 h showed considerably greater differences to the as-sprayed material. The columnar internal structure of the splats was, nevertheless, still nominally retained (see Fig. 15(a)). Again, it is clear that two types of columnar structure may be described: columns that are bounded by pores (seen clearly in the top splat in Fig. 15(a)), and columns that are defined by a difference in crystal orientation to their neighbours (seen in the centre splat of Fig. 15(a)). In the first of these, the columnar width is in the order of 0.7 to 1.5 μm, thereby allowing these columns to be identified with those defined by intercolumnar–columnar porosity in the as-sprayed material. Fig. 15(b) shows at higher magnification a region in the middle of the central splat in Fig. 15(a), i.e. from a region where the columns are thought

(a)

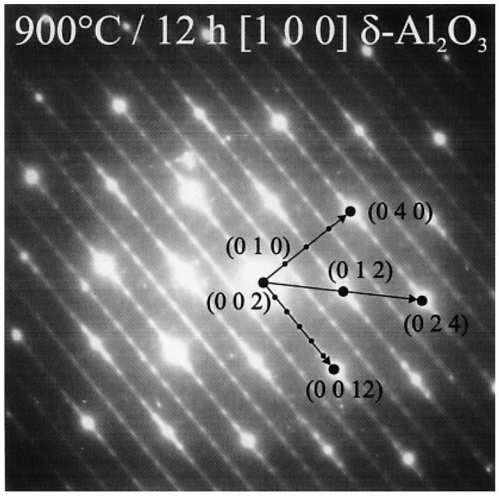

(b)

Fig. 14. (a) TEM micrograph showing the development within individual columns of very fine aligned porosity. The porosity appears to be faceted mirroring the crystallinity of the columnar grain. (b) SAED showing the columns consist of a highly ordered phase. The pattern agrees well with that of a triple stacked spinel type cubic cell of the type reported in literature for δ-Al_2O_3.

to be separated by differences in crystal orientation. There appears to be a further substructure of highly aligned, extremely fine porosity, or voids, inclined at an angle to the axes of the columns. SAED from this area revealed a pattern typical of a very high degree of ordering and corresponding to δ-Al_2O_3.

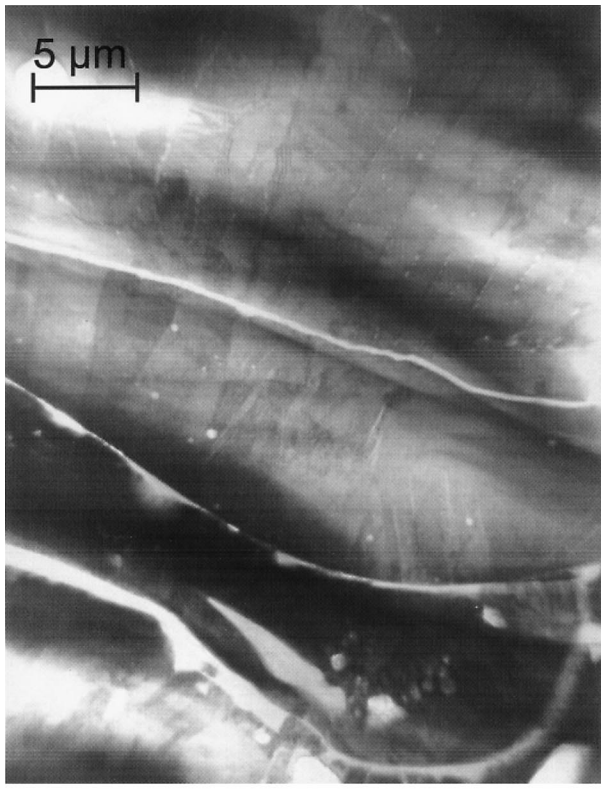

(a)

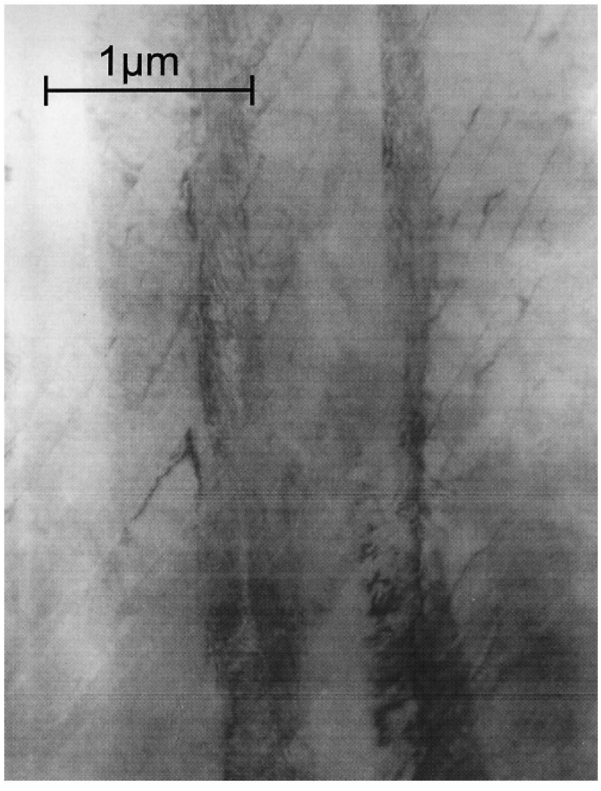

(b)

Fig. 15. TEM micrographs showing (a) the splat internal columnar structure still dominates after heat treatment at 1050°C for 12 h; and (b) at higher resolution, the middle region of the central splat in (a).

The growth and orientation of pores, a process already seen in the material heat treated at 900°C, has progressed to result in a high degree of regimentation. Indeed, the pores are now clearly faceted, mirroring the crystallinity of the surrounding matrix, and, for the first time, they are interconnected with a continuous dislocation line (see Fig. 16).

Two distinct types of structure were revealed within single splats, in neighbouring areas (see, e.g. Fig. 17, which shows the edge of one such splat). The structures previously described as columns are still visible. At higher magnifications areas of high ordering which form domains of between about 10 and 15 nm, may be seen (Fig. 18). This was the most common substructure observed within splats. SAED analysis revealed this structure to be δ-Al_2O_3. Coexisting in neighbouring areas with the domain structure, minor regions of twins could be imaged (Fig. 19). Modulated contrast was received from within the twins, but it was not possible to resolve the contrast sufficiently to show unambiguous internal details. EDX analyses, on the twinned region found no qualitative compositional variation from the neighbouring areas.

3.4.4. Isothermal heat treatments at 1180°C for different times

The heat treatment at 1180°C was chosen on the basis of dilatometry measurements which showed the beginning of

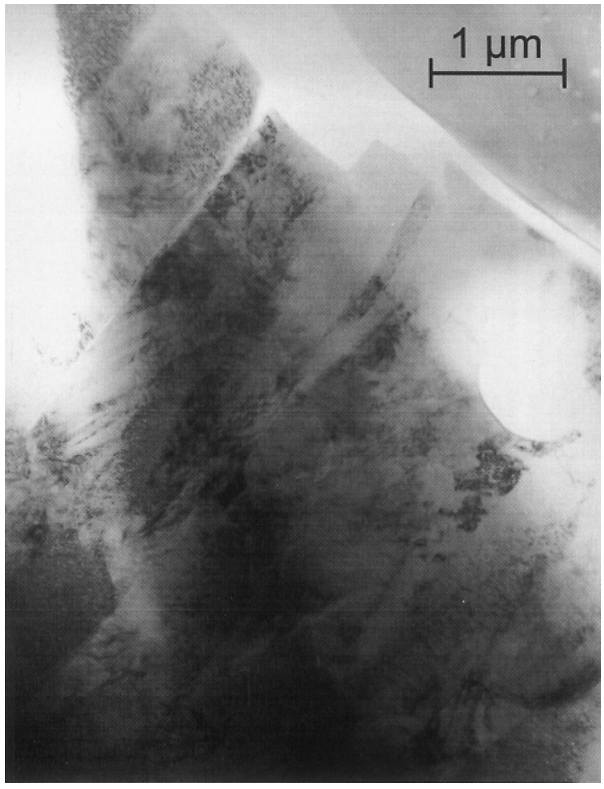

Fig. 17. TEM micrograph of the edge of a splat in material heat treated at 1050°C for 12 h. Areas of twinning and contrast from regions of block domains may be recognised.

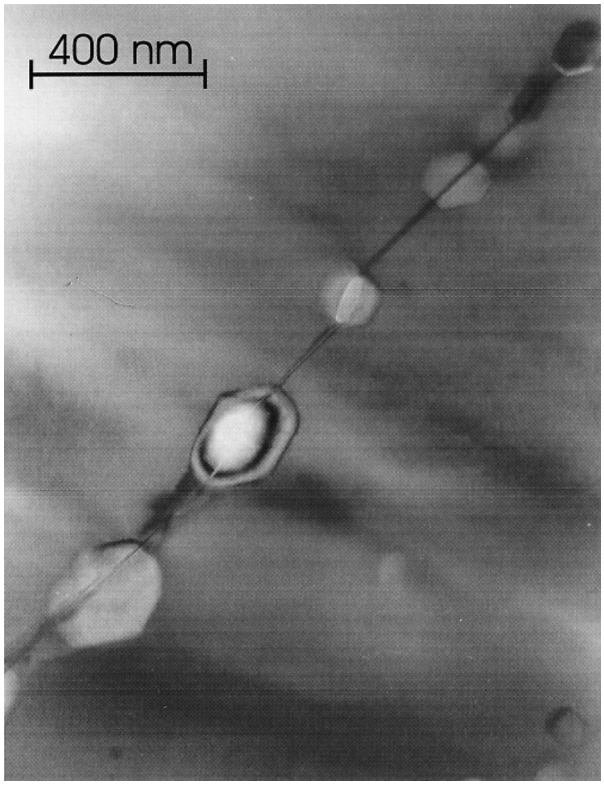

Fig. 16. TEM micrograph showing that the porosity separating the columns in Fig. 15(a) is actually faceted and interconnnected by a continuous dislocation line.

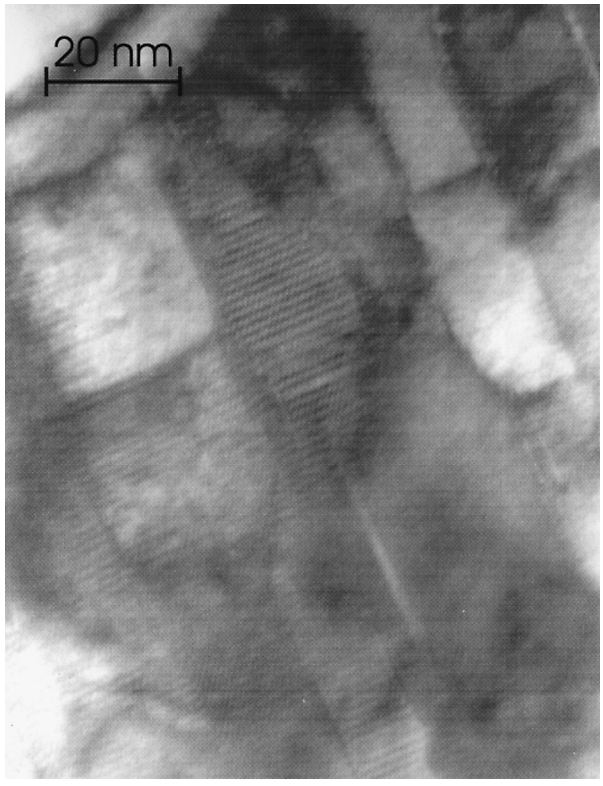

Fig. 18. TEM micrograph showing high resolution image of block domains in δ-alumina.

dimensional instability at about this temperature. Despite the fact that the samples investigated were heated at faster heating rates to avoid spending time at undesired temperatures, this is not entirely avoidable. Furthermore, it should be remembered that transformation rates and times are strongly dependent on heating rate and sample size,[16] so the times given for heat treatment are, in fact, nominal. The final choice of TEM specimens was thus made on the basis of differences in phase composition as detected by XRD (see Fig. 5).

3.4.5. 10 min

The material heat treated for 10 min was already very similar in structure to that treated at 900°C for 12 h. The splats clearly retained their internal columnar substructure and there was no dramatic change from the as-sprayed condition. SAED revealed the development of a considerable amount of δ-Al_2O_3. However, no twinning was observed. There were also very few dislocations and those seen were always in regions of α-Al_2O_3. Nonetheless, much of the smaller scale porosity already exhibited a high degree of faceting.

3.4.6. 20 min

X-ray diffraction showed that the relative amounts of δ-Al_2O_3 (and θ-Al_2O_3) present had both increased, and the amount of γ-Al_2O_3 had decreased after 20 min at 1180°C. There was considerable similarity to material heat treated for 12 h at 1050°C. TEM observation revealed increased ordering and the beginning of the formation of twins. Fig. 20(a) shows one such twin lath nucleating in what was obviously a splat-internal column (identified by comparing the sizes of the structures). The SAED pattern in Fig. 20(b) is taken from the top of the lath containing the twin, and corresponds to

Fig. 19. TEM micrograph showing region of microtwinning in material aged at 1050°C for 12 h. The modulated contrast from within the twin lathes indicates a high density of stacking faults. SAED patterns of this area corresponded most closely to δ-Al_2O_3.

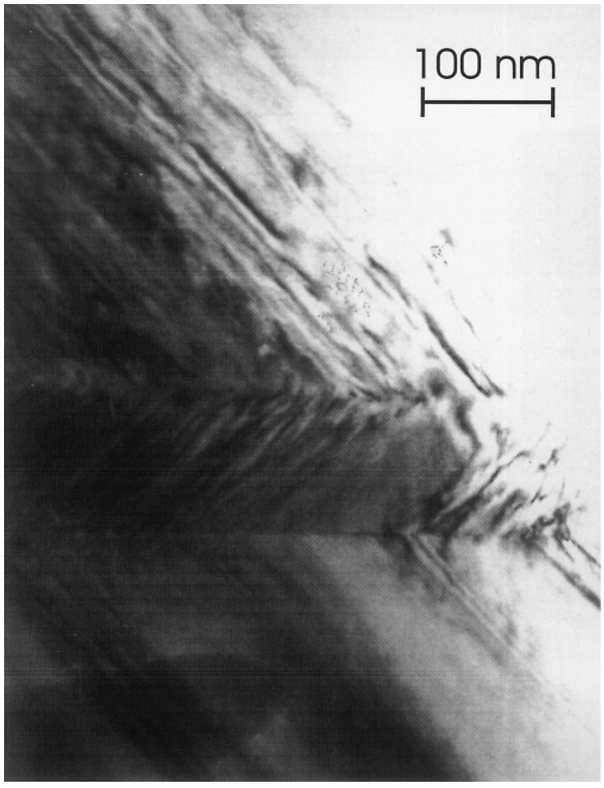

(a)

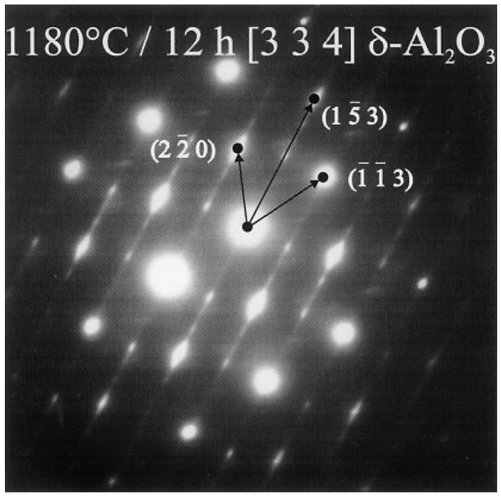

(b)

Fig. 20. (a) TEM micrograph showing the first development of a twin lath within a columnar grain. (b) SAED pattern taken from the column containing the twin lath in (a) showing the [334] zone axis of δ-Al_2O_3.

the [334] zone axis of δ-Al_2O_3. The positions of the spots of maximum intensity agree very well with those in the SAED pattern in Fig. 12(b) lending weight to the argument that the as-sprayed column was γ-Al_2O_3 in the process of transforming to δ-Al_2O_3. SAED from the twin lath, itself, also agreed well with the [334] δ-Al_2O_3 zone axis, indicating that the twins are, at least in the early stages of formation, still δ-Al_2O_3, and not θ-Al_2O_3.

3.4.7. 90 min

The relative amounts of transition aluminas had already reduced after 90 min at 1180°C. Nevertheless, the microstructure and substructure of this material was essentially the same as that for material heat treated at 1050°C for 12 h. Few dislocations were observed.

3.4.8. 3 h

The first major changes in the structure of the material were observed after a heat treatment at 1180°C for 3 h. X-ray diffractometry showed that the relative amounts of δ-Al_2O_3 (and θ-Al_2O_3) had further decreased, accompanied by a definite increase in the amount of α-Al_2O_3.

Although the relative amounts of δ-Al_2O_3 (and θ-Al_2O_3) are seen to decrease, the twin structures are still quite well developed in this material. A region of twins developing from an area of high order is shown in Fig. 21. A block domain structure (which frequently accompanies extreme ordering) is clearly visible, as is a significant amount of aligned and faceted porosity. The porosity is aligned obliquely to the domain or microtwin contrast. Despite the relatively low magnification, the stacking sequence of crystal planes is still visible in some of the domains at the bottom of the figure. This implies the d-spacing of these planes is quite high. Additionally, the facets of the pores seem to have an orientation related to the stacking planes. From the fact that facets of pores in sintered alumina often mirror close packed planes,[38] it may be inferred that the stacking planes are close packed planes of δ-Al_2O_3.

Much of the columnar substructure in the splats had been replaced by a system of self accommodating laths with extensive faceted internal porosity. These laths seem to have retained some resemblance in morphology to their precursor columns. [Nearly identical structures are seen in material heat treated at 1180°C for 12 h (see, e.g. Fig. 22)]. SAED showed these laths to be exclusively α-Al_2O_3. The transformation to α-Al_2O_3 also led to a slight increase in associated dislocation density.

3.4.9. 12 h

The X-ray traces show that after 12 h at 1180°C the material is almost entirely α-Al_2O_3, although remarkably, there is still a trace of δ (or θ) alumina. The columnar

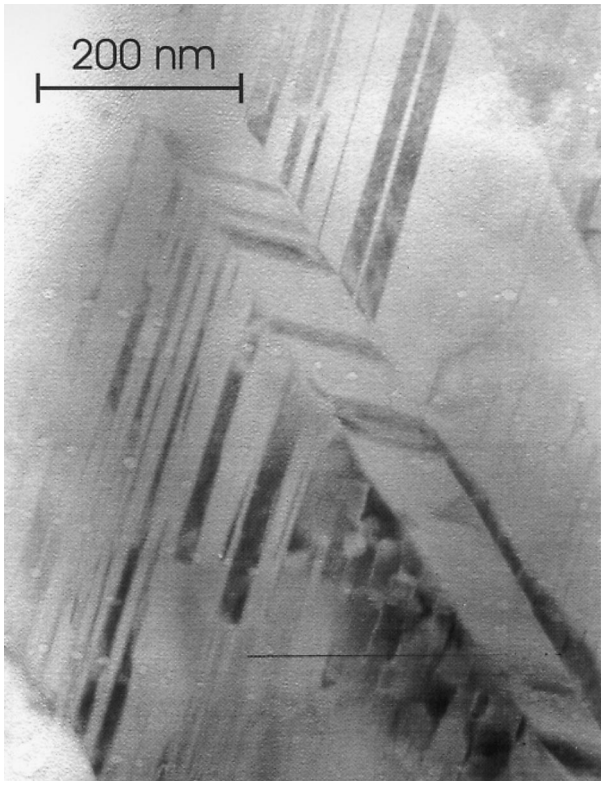

Fig. 21. TEM micrograph showing the development of extensive twinning in a region bounded block domains of highly ordered material.

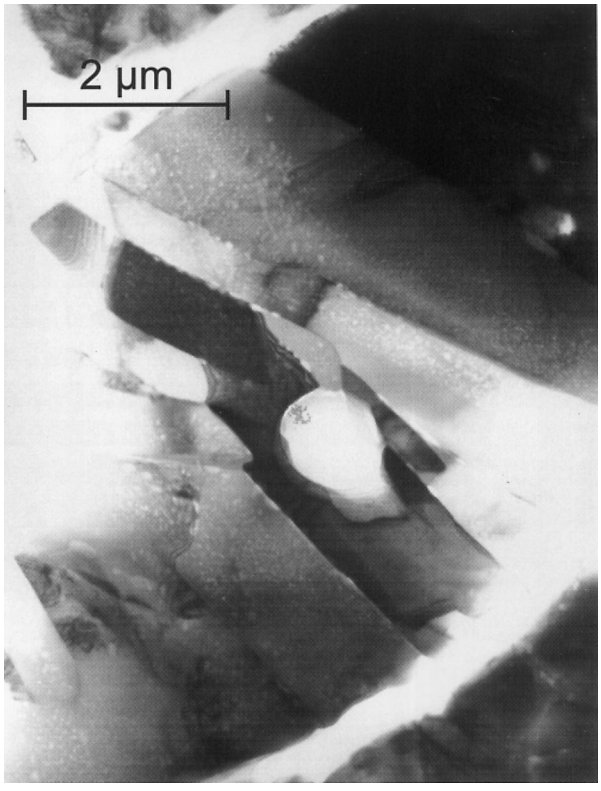

Fig. 22. TEM micrograph of splat after phase transformation to α-Al_2O_3. The previous columnar sub-structure has been replaced by a self accommodating lath structure. This micrograph is taken from material heat treated at 1180°C for 12 h, but similar structures were also visible after 3 h at this temperature. An increase in porosity is identifiable.

substructure typical of the as-sprayed material has been completely replaced by a structure of elongated self-accommodating laths (Fig. 22). The amount of porosity in the new laths has also increased. These new laths are reminiscent of the original columnar substructure, but appear to be inclined at an angle to the original morphological orientation.

Dislocations are far more common in this material than in those heat treated for less time. They may be found interconnecting faceted pores, and in some cases, even form dense networks (see Fig. 23). In general, it seems that this material, after transforming to α-Al_2O_3 undergoes a recovery process to define new grains.

3.4.10. After 12 h at 1550°C

The chosen temperature for this heat treatment is close to the standard sintering temperatures for alumina materials (1600–1700°C).[32] Indeed, SEM investigation indicated that the splats had to some extent sintered together. However, the basic, splat based, quasi-laminated structure of the as-sprayed condition is still dominant (see Fig. 2(b)). The X-ray trace of this material revealed it to be exclusively α-Al_2O_3. There was also significantly more open and closed porosity evident than in the as-sprayed material, present as wide intersplat cavities and equiaxed intrasplat pores and nano-pores.

The most dramatic change in this material is by far the total destruction of the splat-internal columnar structure, or even any related lath-like structure. The splats are now composed of small, slightly elongated grains (about 1×5 μm), with extensive internal porosity, which is both faceted (mirroring crystal orientation) and often aligned. Fig. 24 shows the typical polycrystalline internal composition of a splat. The size of internal porosity is continuously distributed. The smallest identifiable pores are about 10 nm. Some splats are so porous that their internal structure is almost sponge like, reminiscent of the structures seen in transition aluminas after extended dehydroxylation.[39]

The grains also contain a relatively high density of dislocations, which often connect pores in rings, or form dense networks (see, e.g. Figs. 24 and 25). Such pore-dislocation configurations as seen, e.g. in Fig. 25, are common also in conventional high-alumina ceramics.[38,40]

Dense dislocation networks extend laterally across grains and some may form low angle grain boundaries. The SAED pattern in Fig. 26 is taken from a central grain shown in Fig. 24 and shows the [−2−4 1] zone axis of α-Al_2O_3. Traversing the electron beam along the grain axis produced a small shift in the diffraction pattern indicating a slight misorientation down the grain. The low angle grain boundaries form to relieve the strain of this misorientation and are similar to those in

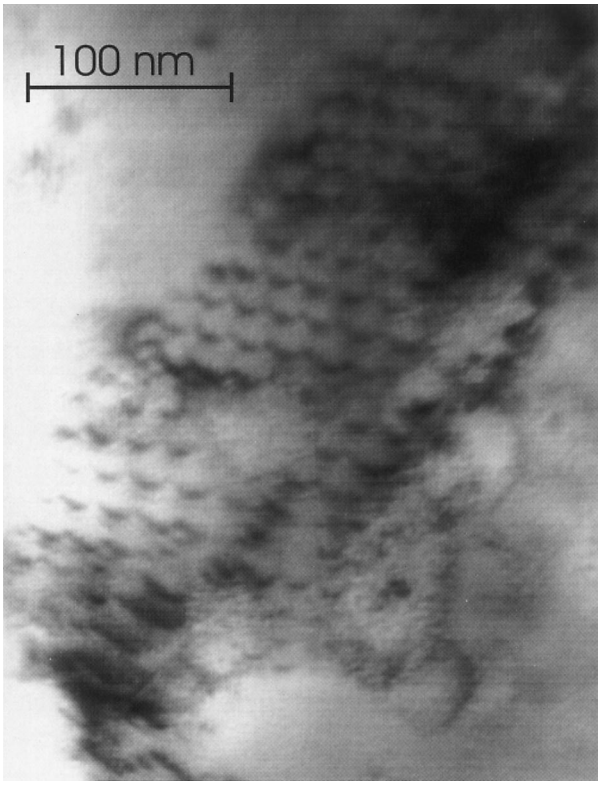

Fig. 23. TEM micrograph of material heat treated at 1180°C for 12 h. Dense networks of dislocations have formed indicating the material is undergoing recovery after transformation.

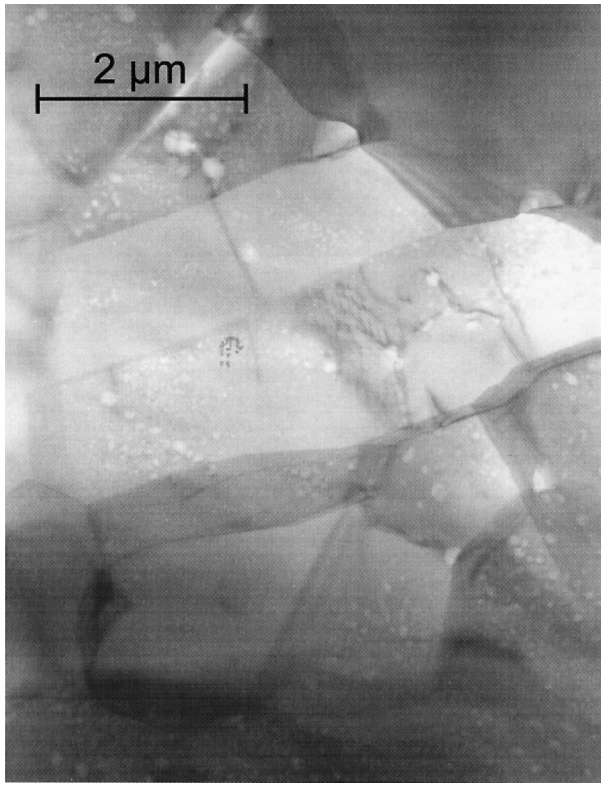

Fig. 24. TEM micrograph showing the internal structure of a splat after heat treatment at 1550°C for 12 h. The material has recrystallised and is fully α-alumina. Elongated grains contain dense dislocation networks and low angle grain boundaries.

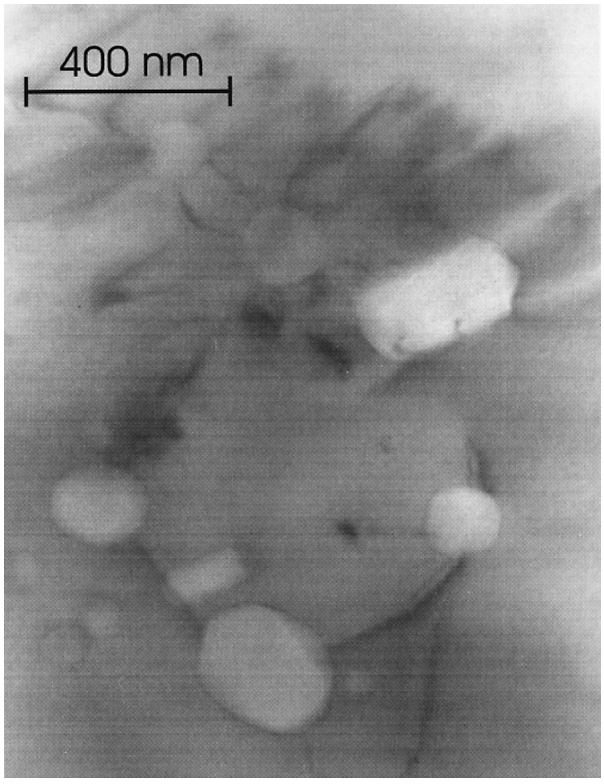

Fig. 25. TEM micrograph showing that the pores in this recrystallised material are also frequently connected by dislocations.

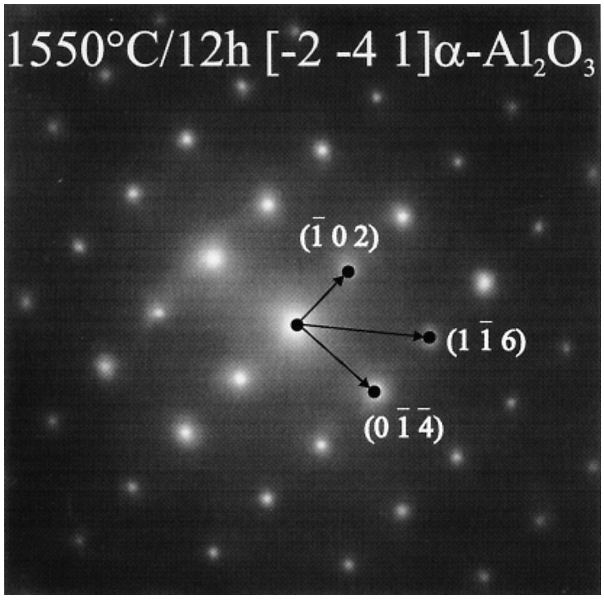

Fig. 26. SAED pattern taken from a central grain in Fig. 24 showing the [−2−4 1] zone axis of α-Al_2O_3.

annealing twins observed in standard alumina materials (see, e.g. Ref. 41).

Essentially, the bulk sprayed alumina after annealing at 1550°C for 12 h is, apart from still possessing a processing related splat structure, and a high degree of transformation related porosity, on a microscale, very similar to other sintered high alumina ceramic materials. Internally, the splats seem to have undergone recovery and recrystallisation.

It should be noted that despite the powder composition, which would normally be expected to result in some glassy phase in a sintered product, all the electron transparent regions investigated yielded well defined SAED patterns. This indicates that there was little, if any, glassy phase in this plasma sprayed alumina.

4. Discussion

Dilatometry has shown that there is little dependence of thermal expansivity (up to the transformation to δ-Al_2O_3) on the alignment of the splats. This implies that a model based on contact ligament expansion would be suitable to describe the initial thermal expansion behaviour of this material.

The temperatures of the maxima of the dilatometry curves, however, do show a dependence on the direction of splat alignment. By extrapolating the expansion curve from before the onset of transformation and taking the difference in thermal strain after transformation, the volume shrinkage on transformation may be estimated at only 2.3 to 2.4%. This compares with an expected theoretical shrinkage of 6.5% for a 65% γ-Al_2O_3 and 35% α-Al_2O_3 material, estimated by rule of mixtures. The lower than expected volume change on phase transformation is confirmed by the RT measurement of permanent shrinkage.

Interpretation of the above data is problematic as little consistent literature is available. Reported values for the density of γ-Al_2O_3 vary from 3.2 g/cm^3 (Refs. 11 and 12), to about 3.67 g/cm^3 (Refs. 1 and 42). The density of θ-Al_2O_3 is reported as 3.56 g/cm^3 in Ref. 11, and that of α-Al_2O_3 varies between 3.95 and 3.99 g/cm^3 in Refs. 1, 42 and 43. In this paper, the ideal density of γ-Al_2O_3 was taken to be 3.55 g/cm^3, since this is close to the reported value for θ-Al_2O_3 and between the extremes.[11], and that of α-Al_2O_3 as 3.95 g/cm^3. This notwithstanding, the results of estimations show the same trends even if the other given values of density are applied.

The lower than expected volume shrinkage could be a result of residual or internal stresses and constraints on morphological rearrangement during phase transformation. For example, the quenched in stresses should be tensile in the plane of splat alignment as they are a consequence of constraints on cooling contraction. This should result in outward directed axial diffusion at elevated temperatures. The α-Al_2O_3 to γ-Al_2O_3 phase change, however, requires a consolidation of matter. Thus, the residual stress would cause directed diffusion during transformation, resulting in the precipitation of radially oriented, aligned internal porosity to compensate

for the opposing requirements. This would lead to a delay in the onset of overall macroscopic shrinkage, and hence the difference in temperature of the peaks of the dilatometry curves. Since crystallographic texture is thought to be absent, such a mechanism would also help explain the striking dependence of the amount of shrinkage observed during transformation to α-Al_2O_3 on splat alignment. TEM evidence which revealed aligned porosity and lath like grains in the α-Al_2O_3 material before recrystallisation supports this postulation.

In the as-sprayed state, the splats have a highly non-equilibrium phase composition and ultra-microstructure. The primary deposited phase in the bulk is a γ or near-γ modification of alumina. Nevertheless, X-ray evidence suggests that all four alumina modifications: γ-Al_2O_3, δ-Al_2O_3, θ-Al_2O_3 and α-Al_2O_3, co-exist in the bulk of the as-sprayed state even though the starting powder was completely α-alumina. During the course of the TEM investigation, however, no θ-Al_2O_3 was uniquely and unambiguously identified in the as-sprayed state.

The dominating splat internal morphology is that of columnar grains indicating high rates of cooling. Since both γ-Al_2O_3 and α-Al_2O_3 may be found as columns of similar size (in neighbouring splats), the cooling rates must have been similar. Generally, it is often assumed that γ-Al_2O_3 nucleates first from the melt. Much of the α-Al_2O_3 present in the as-sprayed material is then formed through a sequence of subsequent transformations according to the Ostwald step rule,[44] i.e. $\gamma \rightarrow \delta \rightarrow \theta \rightarrow \alpha$-$Al_2O_3$. If this is the case, some transformation associated change in the morphology of columns, such as the changes in porosity, twinning or dislocations of the kind observed in artificially aged material would be expected. However, little damage of this kind was observed in the as-sprayed material. Hence, it may be assumed that much of the α-Al_2O_3 nucleated directly from the melt. This would only be possible through heterogeneous nucleation on pre-existing α-Al_2O_3 crystallites which remained in the rapidly and incompletely melted powder stream. This is in agreement with the theories of Plummer and McPherson.[14,45] The formation of the transition alumina phases present in the as-sprayed material may be assumed to be controlled by homogeneous nucleation of γ-Al_2O_3 from the melt and subsequent transformation. The orientation of the splat-internal columns implies that the direction of heat removal is initially perpendicular to the surface of the previous splat. This may result in a portion of the previous splat being reheated, allowing a partial transformation to one of the intermediate phases.

A secondary, yet frequently observed source of α-Al_2O_3 is inclusions of unmelted original powder agglomerate particles (see, e.g. Refs. 19 and 46). Although these particles account for only a little of the α-Al_2O_3 in the material, they may have a significant effect on mechanical properties, because of their loose structure, significantly different morphology, and especially poor interfaces they form with surrounding material. It is probable that these are a result of the atmosphere of gas that the powder particles, being agglomerates, i.e. networks of material and cavities, carry with them.

Despite the poor of contact between powder agglomerate inclusions and impinging splats, the splat internal columnar structure still often forms normal to the surface of the powder. In literature it has often been assumed that in the absence of good contact, the direction of removal of heat is in the plane of the deposit (see, e.g. Refs. 15, 17, 26 and 47). In the present case, however, the tendency for the columnar structure to remain perpendicular to the powder–splat interface strongly suggests that the direction of heat removal remains into the sprayed material, i.e. the powder particle.

Exposure to relatively low temperatures for ceramics (e.g. 900°C), or high temperatures for short time, can lead to substantial changes in phase composition. Progressive increase in order and the eventual formation of block domain and high stacking fault density structures indicates the γ-Al_2O_3 transforms continuously via the short range diffusion and re-ordering of vacancies and cations to δ-Al_2O_3. That many of the SAED patterns can be indexed as both γ-Al_2O_3 and δ-Al_2O_3 suggests that both phases share, to some extent, the same lattice. This seems to remain largely unchanged during this transformation. The evidence supports the mechanism of transformation recently proposed by Wang[48] and Levin,[49] who suggest that the transition aluminas maintain an essentially cubic anion (oxygen) lattice throughout transformation and only vacancies and interstitial (aluminium) cations undergo rearrangement.

The transformation process is accompanied by the segregation and condensation of point defects and vacancies in the bulk and onto pre-existing pores, resulting in an observed increase in splat-internal porosity. Additionally, although the main dehydroxylation of the as-sprayed material is shown by TGA to have occurred on heating between 250 and 390°C, it is also possible that there is also a steady and continuing process of dehydroxylation of the lattice during transition, as there is in transition aluminas formed from boehmite.[39] However, this does not necessarily explain the apparent regimentation of the porosity. The lower than expected loss of water on heat treatment (about 0.4% mass loss as determined by TGA), agrees with the results of the loss-on-ignition tests on transition aluminas reported recently by Zhou.[50] Previous reports led to the expectation of much higher water loss, up to 4.9%. Zhou attributes the discrepancy with the difficulties of accurately calibrating the base line in TGA experiments. However, it also seems logical that the amount of water contained in a transition alumina derived from a hydrated alumina precursor

would differ from that contained in a transition alumina obtained through nucleation and growth from a melt derived from an α-alumina powder.

Prolonged heat treatment below the α-Al_2O_3 transformation temperature results in a wide size distribution of porosity and an increasing number of very small pores only a few nanometres in size, which can only be a consequence of the continuous nucleation of pores. This can lead to a significant increase in the surface area of the material. There is an increase in the size and regularisation of pre-existing porosity, especially that between intrasplat columns. Eventually, faceted porosity interconnected by continuous dislocation lines are formed. Such faceted grain junctions and intragranular pores are, indeed, a common feature of sintered high alumina materials. The faceting is thought to be an equilibrium structure with the faces taking particular crystallographic orientations.[36,38,40] Pore-dislocation assemblies have been observed in other sintered polycrystalline ceramics, where they are often associated with pore–grain-boundary breakaway during sintering. However, in the present case, the heat treatment temperatures are too low to allow macroscopic sintering effects.

As heat treatment continues, the δ-Al_2O_3 orders and in some areas eventually forms a block domain structure within the columns. Locally regions of twins may be observed bounding regions of high ordering. The observed domains (see Fig. 18) agree approximately in size with those reported recently in a modified δ-Al_2O_3 phase thought to have formed by the ordering of vacancies in γ-Al_2O_3.[48] Dauger et al.[51] also observed such domains in plasma sprayed alumina heat treated at 950°C. More recently, however, Levin et al.[49] obtained lattice images of a new polytype of θ-Al_2O_3, formed by the ordering of cations, which revealed the presence of both APB and twin type domain boundaries.

It is possible that the modulated internal contrast observed within twinned regions is a result of microtwinning, i.e. when principle twin laths are themselves internally twinned to produce a *herringbone* structure similar to those seen in other ceramic systems, e.g. in mullite or zirconia.[52] However, since the contrast received was always diffuse and it was not possible to resolve the image into individual twin domains, these must be extremely small. Furthermore, the continuous streaking seen in the SAED patterns of twinned areas, indicates that the modulated contrast more likely results from a very high density of planar defects such as stacking faults. This would be consistent with a high degree of ordering.

It is possible that twins form as a result of the necessity to accommodate lattice strains and minimise stresses which arise from constraints in neighbouring regions as the transformation proceeds locally at different rates. Some stresses and strains may additionally have been quenched in from the spraying process and have a supplementary effect. The observed TEM contrast in regions of twinning is very similar to that observed in martensite laths of various materials, including some ceramics.[53] However, as the twins were formed during an isothermal heat treatment, it is still unclear whether they are formed through short range diffusional rearrangement, i.e. an isothermal decomposition of a parent phase where the product has martensitic characteristics, as may be seen in some materials, or through diffusionless, e.g. dilatational or displacive transformation.[54] The observed sequence of formation of twinned structures confirms the postulation of Bhatkal and Rajan,[55] who reported large scale twinning in a largely δ-alumina material, that such structures are directly a consequence of the transformation process.

It was unfortunately not possible to image the twinned region in high resolution electron microscopy (HREM), and it has not yet been possible to uniquely identify which phase forms these twins. In this investigation the SAED patterns of twinned structures were found to correspond very closely to δ-Al_2O_3. However, as the X-ray traces indicate that this material may contain a little θ-Al_2O_3, and as this was not identified elsewhere, it is possible that the twinned structure is that of the monoclinic θ-Al_2O_3 phase. Multiply twinned structures, identified as θ-Al_2O_3, were also found by Wilson[39] to form during phase transformations on heating boehmite. (It should be noted that the positive and unambiguous identification of θ-Al_2O_3 by electron diffraction requires the application of HREM techniques, since many of the d-spacings in all three transition alurninas considered here are nearly identical[56,57].)

Although at higher temperatures there is some evidence for the formation of θ-Al_2O_3, the relatively small amounts detected implies that the formation of θ-Al_2O_3 does not seem to be a requirement for eventual transformation to the thermodynamically stable α-Al_2O_3 phase. Transformation routes omitting the θ-phase have been reported for plasma-sprayed alurnina with chromia additions,[16] and the formation of θ-Al_2O_3 may be particle size or constraint dependent.[12] Indeed, according to Ref. 57, no conclusive evidence of the necessity for δ-Al_2O_3 to first transform to θ-Al_2O_3 before transforming to α-Al_2O_3 has yet been reported. The apparent continuity of the transformations supports Ervin's postulation[58] that the transition aluminas may be considered order–disorder forms of the same species and Levin's[49] view that δ-Al_2O_3 may be considered a superstructure of γ-Al_2O_3.

The splat internal columnar structure is retained to some extent throughout transformations of the transition aluminas. However, the final transformation to α-Al_2O_3 (at about 1180°C) is reconstructive, requiring the activation of long range diffusion, which is enhanced by the low energy paths offered by dislocations. It results in

the replacement of this structure by a structure of self accommodating lath of fine acicular α-Al_2O_3 grains and is always accompanied by the formation of very finely dispersed, faceted intrasplat pores and the opening of intersplat boundaries. It is possible that the pores nucleate to accommodate the large volume change which accompanies the transformation of transition aluminas to the stable α-Al_2O_3 phase. The internal structure that forms is initially related to the parental columnar structure, which is not surprising as transformation product phases often retain morphological and crystallographic relationships to their parent phases.

Eventually, a recovery structure is formed with dislocation rings and networks forming low angle grain boundaries to accommodate strains arising from constraints and volume change during transformation. Such structures are also common in material after recrystallisation. It is not clear whether these dislocations nucleate due to thermal stresses and migrate to be trapped by pores, or they already exist and pores form on them in consequence of easier diffusion paths offered to defects. The latter scenario is supported by the observation that regions with high dislocation density, e.g. forest dislocations, are often bounded by pore denuded regions.

Despite the activation of long range diffusion, transformation may occur without the onset of large scale sintering between splats, as indicated by the actual increase in porosity. Thus, it is possible to achieve a thermally stable α-Al_2O_3 material which retains an elongated lath internal structure and high intersplat (and intrasplat) porosity.

Extended exposure to temperatures close to standard sintering temperatures (e.g. 1550°C) eventually results in the complete recrystallisation of the internal substructure. The splat internal columnar substructure is completely destroyed. However, the quasi-layered splat structure may be largely retained. The splat internal structure is slightly less porous than just after transformation to α-Al_2O_3. But porosimetry measurements have shown this change to be largely due to a reduction in closed porosity. There is only a small change in the open porosity. Hence, it may be assumed that little macroscopic sintering has taken place. Essentially, the alumina of the splats after recrystallisation may be considered to be the same as conventionally produced alumina.

Four main types of porosity have been identified in the as-sprayed material: (1) large spherical, intrasplat pores which originate from the entrapment of gases in molten particles, and finely distributed, amorphous looking porosity originating from finely dispersed or dissolved gasses in the melt; (2) hemispherical pores resulting from gas trapped between the surface of a solidified splat and an impacting molten or viscous particle; (3) large plate-like intersplat pores resulting from the agglomeration of type 2 porosity, or simply bad splat contact; and (4) thin vertical agglomerations of pores which form between the internal columns of a splat on cooling. The last two types of porosity and, additionally, cracking of columnar interfaces due to thermal or impact stresses are certain to have a profound effect on the strength and fracture behaviour of the as-sprayed material. The results of preliminary investigations into the effects of healing such mechanically weak links have shown that significant improvements in strength and fracture characteristics may be realised.[6,59]

In addition to the morphological classifications of pore types suggested in recent literature, e.g. chamber pores, intersplat pores and vertical cracks,[30,31] it may be possible to facilitate the description of the condition and evolution of a sprayed and annealed alumina by introducing the classification *transformation conditioned porosity* for the in-situ precipitation and changes in morphology of porosity during transformation. This porosity developed on transformation may have a considerable effect on the chemical and mechanical properties of the material. For example, if porosimetry results are taken as absolute, then, despite negligible change in overall porosity up to the reconstructive phase change (as shown in Fig. 7), there is a relative increase of about 0.4% in the amount of open porosity as compared to closed porosity. This small macroscopic change may be estimated to contribute between 1500 and 7500 cm^2/g of new surface area if the new pores are estimated to have diameters of between 10 and 50 nm (see, e.g. Fig. 14(a)). The development of such porosity and the concomitant increase in surface area may significantly effect the chemical activity of such material.

5. Summary and conclusions

Bulk spraying alumina powders results in a material with a quasi-laminated microstructure, consisting primarily of layered splats with a pronounced substructure. Rapid cooling phenomena are responsible for the greater part of the morphology. Post deposition heat treatment causes significant changes in the phase composition and microstructure.

The material in the as-sprayed state consists primarily of metastable γ_{near}-Al_2O_3 (or δ-Al_2O_3) and γ-Al_2O_3 and about 35% thermodynamically stable α-Al_2O_3. The γ_{near}-Al_2O_3 and γ-Al_2O_3 exist as columnar intrasplat grains. Alpha alumina has two sources: it may be found as incompletely melted original powder particles, but the greater part is present as columnar grains which nucleate heterogeneously from seeding α-Al_2O_3 crystallites in the melt. These seeds must be parts of fragmented and incompletely melted original powder particles. The impingement zones between columnar grains within splats are areas of crystallographic mismatch or the agglomeration of porosity, and are likely

to be a source of mechanical weakness. Although some γ-Al_2O_3 may begin to transform in consequence of post deposition heating by subsequent material aggregation, transformation to α-Al_2O_3 after initial deposition is negligible unless external heat treatments are applied.

The thermal expansion coefficient of as-sprayed material increases from 4.5×10^{-6} to 8×10^{-6} K^{-1} for temperatures between 400 and 1000°C, above which the phase change begins to have an ever increasing effect. Thermal expansivity at lower temperatures is not dependent on splat orientation. The onset of transformation to α-Al_2O_3 results in orientationally different rates of shrinkage and material consolidation is about 60% more in the radial (spray) direction as in the axial or tangential (in-plane) directions. The overall shrinkage is much less than expected. This is accounted for by a considerable increase in intrasplat porosity that accompanies transformation. The different residual shrinkage after transformation may be attributed to alignment of this porosity.

Despite the high γ-Al_2O_3 content of the as-sprayed material, the loss of water on heat treatment (0.4% mass loss) is less than would be expected when compared to a boehmite derived γ-Al_2O_3. It is thought probable that the water content of γ-Al_2O_3 which nucleated and grew from a melt is different to that derived from mineral precursors.

The phase transformation from γ to δ-Al_2O_3 is a continuous order–disorder transformation. Although some θ-Al_2O_3 was detected in the heat treated material, no conclusive evidence was found for the necessity for γ-Al_2O_3 to pass through the whole transition transformation sequence, i.e. $\gamma\rightarrow\delta\rightarrow\theta\rightarrow\alpha$-$Al_2O_3$. It is likely that the γ-Al_2O_3 can transform to α-Al_2O_3 via only the δ-Al_2O_3 intermediate. The high degree of order required by the later stages of transformation leads to the formation in the microstructure of block domains and regions of twinning. HREM would be required for unique and unambiguous identification of the phase systems formed.

During transformation through the transition aluminas there is a steady and continuous precipitation of fine nano-sized porosity as a result of the ordering process and consolidation of defects in the material. This increase is not reliably determinable by Archimedean porosimetry due to the insensitivity of this technique to changes in closed porosity if these are accompanied by changes in the density of the solid. The interpretation of Archimedean porosimetry is, in any case, difficult due to inconsistent literature data on ideal densities. Furthermore, it has been shown that Archimedean porosimetry can deliver consistent and reliable estimations of closed and open porosity only if immersion times are sufficiently long to allow penetration of extremely narrow cavities. Overnight soaking under light vacuum, a commonly applied experimental procedure, does not fulfil this requirement.

The columnar substructure of the splats is maintained throughout the transition phase changes and is nominally present even after the final reconstructive transformation to α-Al_2O_3. The transformation to α-Al_2O_3 takes place at about 1180°C. The rates of transformation are not necessarily fast and residual transition phases may be found even after 12 h at this temperature. A significant jump in open and closed porosity is associated with this phase change, despite macroscopic shrinkage.

Further heat treatment close to sintering temperatures can lead to the recovery and recrystallisation of the splat internal microstructure. This process results in a significant increase in the mechanical integrity of splats. It is also associated with a slight drop in the amount of closed porosity whereas the open porosity remains unchanged. Little macroscopic sintering takes place even after 12 h at 1550°C.

The consolidation of material defects, the need to minimise stresses caused by constraints and, probably, continuing dehydroxylation during the transformation process lead to the formation of very finely dispersed, faceted internal porosity and eventually the appearance of dislocation rings and networks. Dislocations provide easy diffusion paths and therefore play an important role in microstructural development.

In addition to commonly used morphological classifications of porosity a new classification *transformation conditioned porosity* may be applied to describe the evolution of the material during heat treatment.

The systematic heat treatment of a plasma sprayed alumina may be used to obtain materials with a variety of phase compositions and ultra-microstructures. It is possible to obtain thermally stable plasma sprayed aluminas (approx. 100% α-Al_2O_3) with greatly differing ultra-microstructures, whilst largely retaining their characteristic quasi layered splat structure. Different heat treatments should result in materials with different mechanical properties.

The investigation of the effects of heat treatment on mechanical properties of plasma sprayed alumina is the subject of a future work.

Acknowledgements

This work was partially funded by the Austrian Ministry for Science and Transport under the contract no. GZ 140.539/3-V/6/98. The authors would also like to express their thanks and appreciation to Dr. E.H. Lutz (formerly) of LWK-Plasmakeramik, Gummersbach, Germany; Dr. Warbichler and Dr. Hofer of the Forschungsinstitut für Elektronenmikroskopie of the Technical University, Graz, Austria; and Mr. J. Towner of the Department of Materials Science and Engineering of the University of Surrey, Guildford, UK.

References

1. Pawlowski, L., *The Science and Engineering of Thermal Spray Coatings*. Wiley, Chichester, 1995.
2. Anon. *Thermal Spray Coatings: Properties, Processes and Applications*. Proc. 4th Nat. Thermal Spray Conf., Pittsburgh, PA, 4–10 May 1991. ASM International, Materials Park, OH, 1992.
3. Heimann, R. B., *Plasma-Spray Coating: Principles and Applications*. VCH, Weinheim/New York, 1996.
4. Lugscheider, E. et al., Quo vadis, thermal spray technology? *Powder Metallurgy Int*., 1991, **23**, 33–39.
5. Lutz, E. H., Microstructure and properties of plasma ceramics. *J. Am. Ceram. Soc*., 1994, **77**, 1274–1280.
6. Damani, R. J. and Lutz, E. H., Microstructure, strength and fracture characteristics of a free standing plasma-sprayed alumina. *J. Eur. Ceram. Soc*., 1997, **17**, 1351–1359.
7. Wang, D. and Berndt, C. C., Anisotropic thermal expansion behaviour of thermally sprayed coatings. In *2nd Plasma-Technik-Symp., Vol. 2*, Lucerne, 1991. Wohlen, Switzerland, 1991, pp. 295–304.
8. Lutz, E. H., Crack resistance anisotropy in plasma-sprayed ceramic composites. *Fachberichte der DKG*, 1995, **72**, 713–716.
9. Thompson, V. S. and Whittemore, O. J. Jr., Structural changes on reheating plasma-sprayed alumina. *Cer. Bull*., 1968, **47**, 637–641.
10. Travitzky, N. A., Brandon, D. G. and Gutmanas, E. Y., Toughening of commercial 86 wt.% Al_2O_3 by controlled heat treatments. *Materials Science and Engineering*, 1985, **71**, 65–70.
11. Gitzen, W. H., *Alumina as a Ceramic Material* (Special publication no. 4). The American Ceramic Society, Westerville, OH, 1970.
12. Wefers, K. and Misra, C., Oxides and hydroxides of aluminium. Alcoa technical paper no. 19, revised. Alcoa Laboratories, 1987.
13. McPherson, R., Formation of metastable phases in flame and plasma-prepared aluminia. *J. Mat. Sci*., 1973, **8**, 851–858.
14. McPherson, R., On the formation of thermally sprayed alumina coatings. *J. Mat. Sci*., 1980, **15**, 3141–3149.
15. Safai, S., A microstructure investigation of plasma sprayed metal and oxide coatings. Doctoral thesis, State University of New York at Stony Brook, New York, 1979.
16. Ilavsky, J., Studies of plasma sprayed alumina. Doctoral thesis, State University of New York at Stony Brook, New York, 1994.
17. Safai, S. and Herman, H., Plasma-sprayed materials. In *Treatise on Materials Science and Technology*, Vol. 20, ed. H. Herman. Academic Press, New York, 183–213.
18. Sampath, S. and Herman, H., Microstructural development of plasma sprayed coatings. In *Proc. 12th Int. Thermal Spraying Conf*., London, 1989, pp. 247–256.
19. McPherson, R., The relationship between the mechanism of formation, microstructure and properties of plasma sprayed coatings. *Thin Solid Films*, 1981, **83**, 297–310.
20. Kudinov, V. V., Pekshev, P. Yu. and Safiullin, V. A., Forming of the structure of plasma-sprayed materials. In *High-Temperature Dust-Laden Jets in Plasma Technology*, ed. O. P. Solonenko and A. I. Fedorchenko. VSP, Utrecht, The Netherlands, 1990, pp. 381–418.
21. Pekshev, P. Yu and Safiullin, V. A., Porosity of plasma sprayed alumina. In *High-Temperature Dust-Laden Jets in Plasma Technology*, ed. O. P. Solonenko and A. I. Fedorchenko. VSP, Utrecht, The Netherlands, 1990, pp. 437–462.
22. Wilms, V. and Herman, H., Crystallography and microstructure of equilibrium and metastable phases resulting from plasma spraying of ceramic coatings. Proc. 8th Int. Thermal Spray Conf., FL, 1976, pp. 236–243.
23. Pawlowski, L., Microstructural study of plasma sprayed alumina and nickel–chromium coatings. *Surface and Coatings Technology*, 1987, **31**, 103–116.
24. Safai, S. and Herman, H., Plasma sprayed coatings: their ultra-microstructure. In *Advances in Surface Coating Technology — International Conference, London, 1978*, pp. 1–13.
25. Guilemany, J. M., Nutting, J. and Dougan, M. J., A transmission electron microscopy study of the microstructures present in alumina coatings produced by plasma spraying. *J. Thermal Spray Technology*, 1997, **6**, 425–429.
26. Braue, W. *et al*., In-plane microstructure of plasma-sprayed Mg–Al spinel and 2/1-mullite based protective coatings: an electron microscopy study. *J. Eur. Ceram. Soc*., 1996, **16**, 85–97.
27. McPherson, R. and Shafer, B. V., Interlamellar contact within plasma-sprayed coatings. *Thin Solid Films*, 1982, **97**, 201–204.
28. Wilms, V. and Herman, H., Plasma spraying of Al_2O_3 and Al_2O_3–Y_2O_3. *Thin Solid Films*, 1976, **39**, 251–262.
29. Stevens, R. and Harmsworth, P. D., Microstructure of zirconia–yttria plasma-sprayed thermal barrier coatings. *J. Mat. Sci*., 1992, **27**, 616–624.
30. Kuroda, S., Properties and characterisation of thermal sprayed coatings — a review of recent research progress. In *Thermal Spray: Meeting the Challenges of the 21st Centur*y, ed. Ch. Coddet. Proc. 15th Int. Thermal Spray Conf., 25–29 May 1998, Nice. ASM International, Materials Park, OH, 1998, pp. 539–550.
31. Li, C. J., He, Y. and Ohmori, A., Characterisation of structure of thermally sprayed coatings. In *Thermal Spray: Meeting the Challenges of the 21st Century*, ed. Ch. Coddet. Proc. 15th Int. Thermal Spray Conf., 25–29 May 1998, Nice. ASM International, Materials Park, OH, 1998, pp. 717–722.
32. Morrell, R., *Handbook of Properties of Technical & Engineering Ceramics, Part 2: Data Reviews, Section 1: High-Alumina Ceramics*. HM Stationary Office, London, 1987.
33. Whittemore, O. J. Jr. and Ault, N. N., Thermal expansion of various ceramic materials to 1550°C. *J. Am. Ceram. Soc*., 1956, **39**(12), 443–444.
34. Houben, G. M. M. and De Boer, J. H., Constitution of γ-alumina. Trans. Int. Ceram. Congr., 3rd Congress, Paris, 1952, pp. 77–79.
35. Yanagida, H. and Yamaguchi, G., Thermal effects in the lattices of η- and γ-aluminimum oxide. *Bull. Chem. Soc. Japan*, 1965, **38**, 2194–2196.
36. Lippens, B. C. and De Boer, J. H., Study of phase transformations during calcination of aluminium hydroxides by selected area electron diffraction. *Acta. Crystr*., 1964, **17**, 1312–1321.
37. Rooksby, H. P. and Rooymans, C. J. M., The formation and structure of delta alumina. *Clay Minerals Bull*., 1961, **4**, 234–238.
38. Powell-Dogan, C. A. and Heuer, A. H., Microstructure of 96% alumina ceramics: I, characterization of the as-sintered materials. *J. Am. Ceram. Soc*., 1990, **73**, 3670–3676.
39. Wilson, S. J., Phase transformations and development of microstructure in boehmite-derived transition aluminas. *Proc. Brit. Ceram. Soc*., 1979, **28**, 281–294.
40. Powell-Dogan, C. A. and Heuer, A. H., Microstructure of 96% alumina ceramics: III, crystallization of high-calcia boundary glasses. *J. Am. Ceram. Soc*., 1990, **73**, 3684–3691.
41. Shiue, Y. R. and Phillips, D. S., The crystallography of annealing twins in alumina ceramics. *Phil. Mag. A*, 1984, **40**, 677–702.
42. Wu, Sh. J., De Jonghe, L. C. and Rahaman, M. N., Sintering of nanophase γ-Al_2O_3 powder. *J. Am. Ceram. Soc*., 1996, **79**, 2207–2211.
43. Huffadine, J. B. and Hollands, E. J., Flame spraying of ceramic materials. British Patent 903,709, 15 August 1962.
44. Ostwald, W., Studien über die Bildung und Umwandlung fester Körper, 1. Abhandlung: Übersättigung und Überkaltung. *Z. Physik. Chemie*, 1897, **22**, 289–330.
45. Plummer, M., The formation of metastable aluminas at high temperatures. *J. Appl. Chemistry*, 1958, **8**, 35–44.

46. Ramm, D. A. J. et al., Correlations between spraying conditions and microstructure for alumina coatings produced by HVOF and VPS. In Proc. 7th Nat. Thermal Spray Conf., 20–24 June 1994, Boston, MA, pp. 239–244.
47. Herman, H., Plasma sprayed coatings. *Scientific American*, 1988, September, 112–117.
48. Wang, Y. G. et al., Ordering of octahedral vacancies in transition aluminas. *J. Am. Ceram. Soc.*, 1998, **81**, 1655–1660.
49. Levin, I. et al., Cubic to monoclinic phase transformations in alumina. *Acta. Mater.*, 1997, **45**, 3659–3669.
50. Zhou, R.-Sh. and Snyder, R. L., Structures and transformation mechanisms of the η, γ, and θ transition aluminas. *Acta Cryst. C*, 1991, **47**, 617–630.
51. Dauger, A., Fargeot, D. and Laval, J. P., Metastable phases of alumina. In *Mat. Res. Soc. Symp. Proc.*, Vol. 21. Elsevier, 1984, pp. 207–211.
52. Amelinckx, S., Gevers, R. and Van Landugt, J. (eds), *Diffraction and Imaging Techniques in Material Science, Vol. 1: Electron Microscopy*. North-Holland, 1978.
53. Muddle, B. C. and Hugo, G. R., Martensitic transformations in ceramics. In *Proc. Int. Conf. on Martensitic Transformations 1992*. Monterey Institute for Advanced Studies, Monterey, CA, 1993, 647–658.
54. Rao, C. N. R. and Rao, K. J., *Phase Transitions in Solids*. McGraw-Hill, New York, 1978.
55. Bhatkal, R. M. and Rajan, K., Enhancement of heat exchanger surfaces: interfacial reactions during thermal spraying. In Proc. 7th Nat. Thermal Spray Conf., 20–24 June 1994, Boston, MA, pp. 141–146.
56. Morrissey, K. J. *et al.*, Transition alumina structures studied using HREM. *Ultramicroscopy*, 1985, **18**, 379–386.
57. Levin, I. and Brandon, D., Metastable alumina polymorphs: crystal structures and transition sequences. *J. Am. Ceram. Soc.*, 1998, **81**, 1995–2012.
58. Ervin, G., Structural interpretation of the diaspore-corundum and boehmite-γ-Al_2O_3 transitions. *Acta Cryst.*, 1952, **5**, 103–108.
59. Damani, R. J., Mechanical and microstructural characterisation of a free standing plasma-sprayed alumina. In *Thermal Spray: Meeting the Challenges of the 21st Century*, ed. Ch. Coddet. Proc. 15th Int. Thermal Spray Conf., 25–29 May 1998, Nice. ASM International, Materials Park, OH, 1998, pp. 1217–1222.